Thesis

Theoretical Studies on Electronic Properties of Organic Conductors

Yutaka Imamura

Department of Functional Molecular Science
School of Mathematical and Physical Science
The Graduate University for Advanced Studies

Contents

Chapter 1.

Introduction

The organic conductor, TTF-TCNQ synthesized in 1973 gathered much attention because of its high electrical conductivity [1]. After this discovery, many other organic conductors have been synthesized and studied. They show interesting phases, e.g., superconductivity (SC), charge density wave (CDW), spin density wave (SDW) and antiferromagetic (AF) states. These physical properties are controlled by dimensionality, electron correlation and electron-lattice interaction. The physical parameters can be changed by chemical modification, pressure and temperature. Therefore modifying the organic molecules chemically, we can investigate the roles of constituting atoms and molecules experimentally. From the viewpoint of the molecular-design, organic conductors are of great importance.

Representative one-dimensional (1-D) organic conductors are TTF-TCNQ, $(TMTSF/TMTTF)_2X$ (X=PF_6, AsF_6, ClO_4, etc) and $(DCNQI)_2X$ (X=Ag, Li, DCNQI= 2,5-disubstituted N,N'-dicyanoquinonediimine) salts whose organic molecules are stacked one-dimensionally. Those materials show the unique low-dimensional characters. For example, TTF-TCNQ has a Fermi surface instability due to the 1-D character of electronic states. Actually, for TTF-TCNQ, the electronic system becomes a CDW state at low temperatures because of its instability [2]. For $(TMTTF)_2PF_6$ salt, the ground state becomes a spin-Peierls (SP) state, but applying pressure, the electronic state becomes a SDW state. On the other hand, $(TMTSF)_2PF_6$ shows superconductivity under applied pressure at around 1 K [3]. The complex phase of $(TMTTF/TMTSF)_2X$ as a function of effective pressure is discussed in Ref. [4]. Representative 2-D organic conductors are BEDT-TTF and dmit salts. Especially, the κ-$(BEDT\text{-}TTF)_2X$ (BEDT-TTF=bis(ethlenedithio)tetrathiafulvalene) salts have a 2-D character, and therefore the nesting of Fermi surface is not effective. Among BEDT-TTF salts, κ-type salts have the highest T_c. β,β'-$Me_4Z[Pd(dmit)_2]_2$ (Z= N, P, As, and Sb) show various physical properties by changing pressure, temperature, a choice of cation and so on [5]. The two bands which have different characters in dimension contribute to the conduction, and their characters can be controlled by changing effective pressure. In this thesis, we focus

on the κ-BEDT-TTF salts and DCNQI salts.

(R1, R2-DCNQI)$_2$M salts (see Fig. 1.1) have unique physical properties. DCNQI-Ag/Li salts show a strong 1-D character of conductivity which originates from 1-D columns consisting of face to face stacking of DCNQI molecules. However, for M=Cu, the hybridization between a *d* orbital of Cu and a π orbital of DCNQI destroys the 1-D character. Therefore, even at low temperatures, some of DCNQI-Cu salts are metallic [6]. The DCNQI salts are the tetragonal crystals of space group $I4_1/a$ as shown in Fig. 1.2 [7,8]. For M=Li,Ag, the formal charges of DCNQI and M are −1/2 and +1, respectively [9], on the other hand, for M=Cu, those of DCNQI and M are −2/3 and +4/3, respectively [10]. The conduction electrons therefore form a 1-D band with 1/4 and 1/3 fillings, respectively. The physical properties of DCNQI salts are strongly influenced by substituents, R1 and R2 (see Fig. 1.3). For example, the ground state of (DI-DCNQI)$_2$Ag salt becomes the $4k_F$ CDW of the charge modulation type below 200 K and becomes an AF state at 5.5 K, as observed by Hiraki and Kanoda [11,12]. The ground state of (DMe-DCNQI)$_2$Ag salt is the $4k_F$ CDW with lattice distortion below 100 K. It becomes a spin-Peierls state at 80 K [13]. For DCNQI-Cu salts, the electronic states which change from metals to insulators at low temperatures due to substituent effects is understood in terms of the amount of charge transfer from Cu to DCNQI [14]. Thus, the physical properties are very sensitive to the substituents of DCNQI molecules, which can be easily modified or synthesized experimentally.

From theoretical point of view, various studies have been carried out for DCNQI-M (M=Cu, Ag and Li) salts [15-28]. Seo and Fukuyama calculated the electronic states of the 1-D quarter-filled band by the Hartree-Fock (HF) approximation [15]. They concluded that the nearest-neighbor Coulomb interactions introduce charge disproportionation. Kobayashi *et al.* also used the HF model to a similar electronic system, (TMTSF)$_2$PF$_6$, and investigated the coexistence of the $2k_F$ SDW and $2k_F$ CDW states considering the electron-lattice interaction and the next-nearest-neighbor Coulomb interaction [16,17]. For DCNQI-Cu salts, Suzumura and Fukuyama employed

a periodic Anderson model including the electron-phonon interactions and studied physical properties in the framework of the mean field theory [18]. Ogawa and Suzumura applied the slave boson method to the same model and examined the effect of strong correlation on the metal-insulator transition [19-24]. Miyazaki *et al.* calculated the metallic states of DCNQI-Ag, Li, Cu salts using the local density approximation and generalized gradient approximation (LDA and GGA) based on the density functional theory (DFT) [25-27]. They obtained the first-principles Fermi surfaces and dispersions of the DCNQI-Cu/Ag salts. This problem was also studied by Yonemitsu from the renormalization-group approach [28].

BEDT-TTF shown in Fig. 1.4 is a donor molecule which makes various kinds of charge transfer crystals distinguished by α-, β-, κ-, etc, phases. Among them, the κ-BEDT-TTF salts are composed of two dimensional donor sheets in which paired BEDT-TTF molecules are arranged almost orthogonal to each other (see Fig. 1.5). The formal charges of the BEDT-TTF molecule and the counter-ion are +1/2 and -1, respectively. The space group of κ-(BEDT-TTF)$_2$Cu[N(CN)$_2$]X (X=Cl, Br and I) is Pnma. At ambient pressure, the κ-(BEDT-TTF)$_2$Cu[N(CN)$_2$]Br salt shows superconductivity below T_c= 11.6 K, whereas κ-(BEDT-TTF)$_2$Cu[N(CN)$_2$]Cl is a Mott insulator with the AF ordering as shown in Fig 1.6 [29,30]. However, under 0.3 kbar, the latter becomes a superconductor with T_c= 12.8 K. On the other hand, κ-(BEDT-TTF)$_2$Cu[N(CN)$_2$]I does not show superconductivity. Electronic properties of the BEDT-TTF salts are therefore very sensitive to pressure and counter-anion.

Various theoretical studies have been done for the BEDT-TTF salts [31-49]. From the first-principles approach, Xu *et al.* calculated the Fermi surface of κ-(BEDT-TTF)$_2$Cu(NCS)$_2$ with use of the LDA based on the DFT [31]. From ab initio molecular orbital (MO) theory, Demiralp and Goddard optimized the BEDT-TTF monomer at HF/6-31G** and studied the physical properties using the 2-D Hubbard model within the HF approximation [32-36]. Kino and Fukuyama adopted the same model and explained different physical properties of κ-(BEDT-TTF)$_2$X, α-(BEDT-TTF)$_2$I$_3$ and

$(BEDT\text{-}TTF)_2MHg(SCN)_4$ by using a couple of key parameters, the band overlap and the dimerization [37-39]. Fortunelli and Painelli described the ab initio evaluation of Hubbard parameters for the BEDT-TTF dimer unit and calculated those of the κ-$(BEDT\text{-}TTF)_2Cu[N(CN)_2]Br$ salt [40-43]. Okuno and Fukutome showed an effective Hamiltonian of β- and κ-phases and concluded that the electron correlation is very strong [44]. The nesting and pressure effect of the Fermi surface were discussed [45,46]. Using the dimer Hubbard model within the spin fluctuation exchange (FLEX) approximation, the pairing symmetry and the superconducting transition, T_c, were studied [47-49].

For both the DCNQI and BEDT-TTF salts, there are many theoretical studies, mainly band calculations and model analyses, which were explained above. Although the components of the conductors are organic molecules, to which ab initio methods have been successfully applied, there has been no quantitative study of bulk properties based on the ab initio MO theory. The purpose of this thesis is to clarify the electronic properties started from the ab initio MO theory. This will be of great importance for designing organic conductors since their electronic states are very sensitive to the constitution and arrangement of organic molecules. Now, thanks to recent developments of computer and algorithmic technology, ab initio method becomes a powerful tool to obtain the detailed information of electronic states of large molecules. We perform ab initio MO calculations of DCNQI and BEDT-TTF molecules and study the electronic properties of organic molecules. Based on those results, we construct effective Hamiltonian of finite cluster model and calculate its ground and low-lying excited states by the exact diagonalization. The electronic phases of the obtained states are analyzed by spin correlation functions.

The previous 2-D Hubbard model calculations included only the on-site Coulomb effects [35,37-39]. However, Seo and Fukuyama, and Kobayashi *et al.* suggested the importance of long-range Coulomb interactions. Therefore we adopt the 2-D extended Hubbard model including long-range as well as on-site Coulomb interactions and

calculate its ground state within the HF approximation.

The organization of this thesis is as follows. In chapter 2, we explain the theoretical treatment of organic conductors. In chapters 3 and 4, we discuss electronic properties of DCNQI and BEDT-TTF salts, respectively. The conclusion is given in chapter 5.

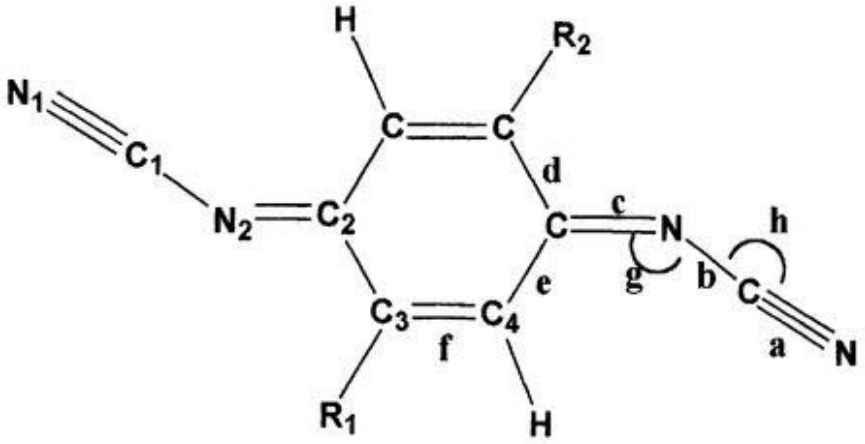

Fig. 1.1. The molecular structure of the 2,5-R1,R2-DCNQI molecule.

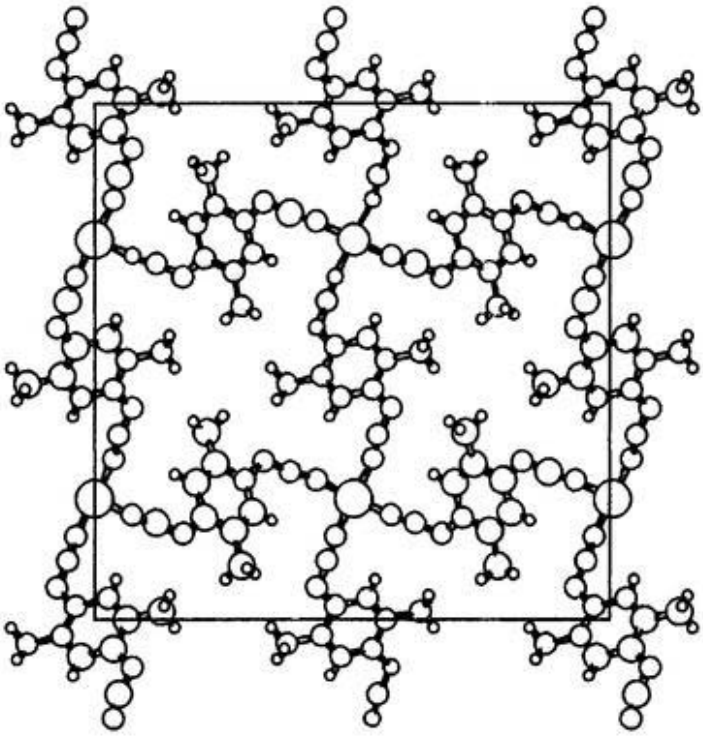

Fig. 1.2. The c-axis projection of the crystal structure of the $(R1,R2\text{-}DCNQI)_2M$ (M=Ag,Li, Cu) salts.

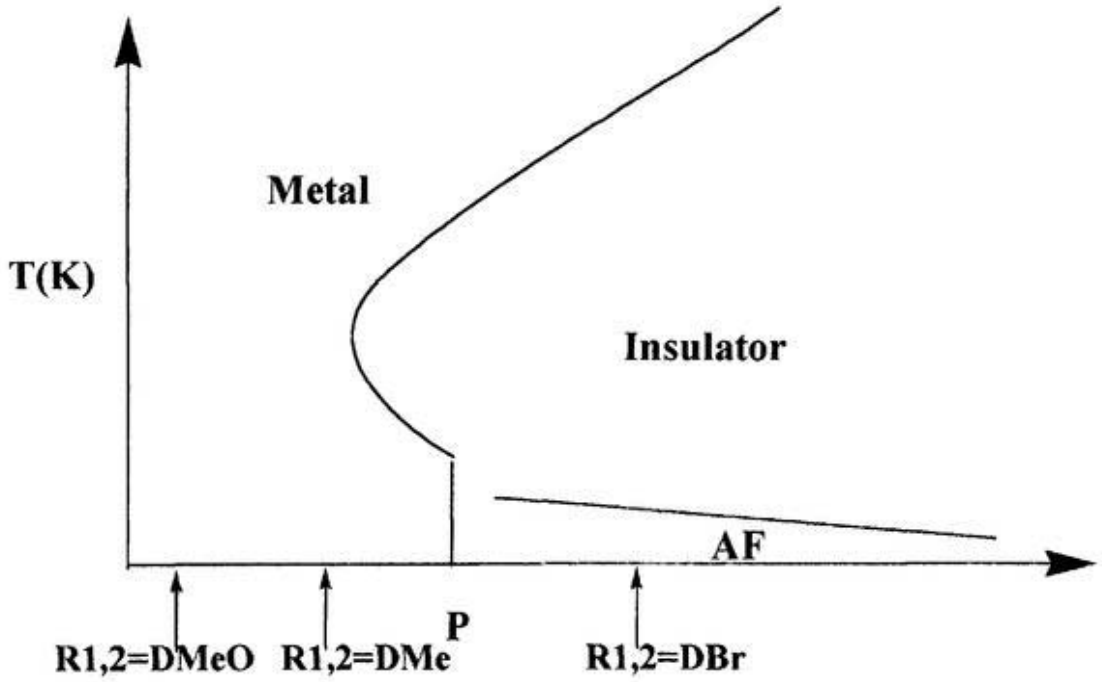

Fig. 1.3. An experimental phase diagram of the (R1,R2-DCNQI)$_2$Cu salts on a plane of pressure (P) and temperature (T).

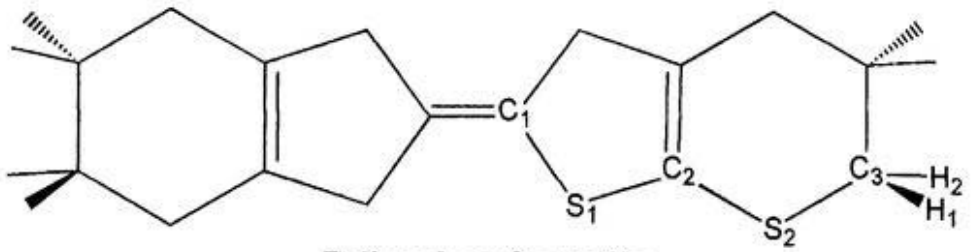

Eclipsed conformation

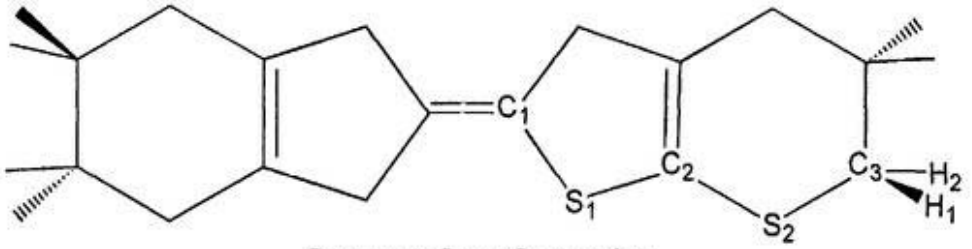

Staggered conformation

Fig. 1.4. The molecular structure of the BEDT-TTF molecule.

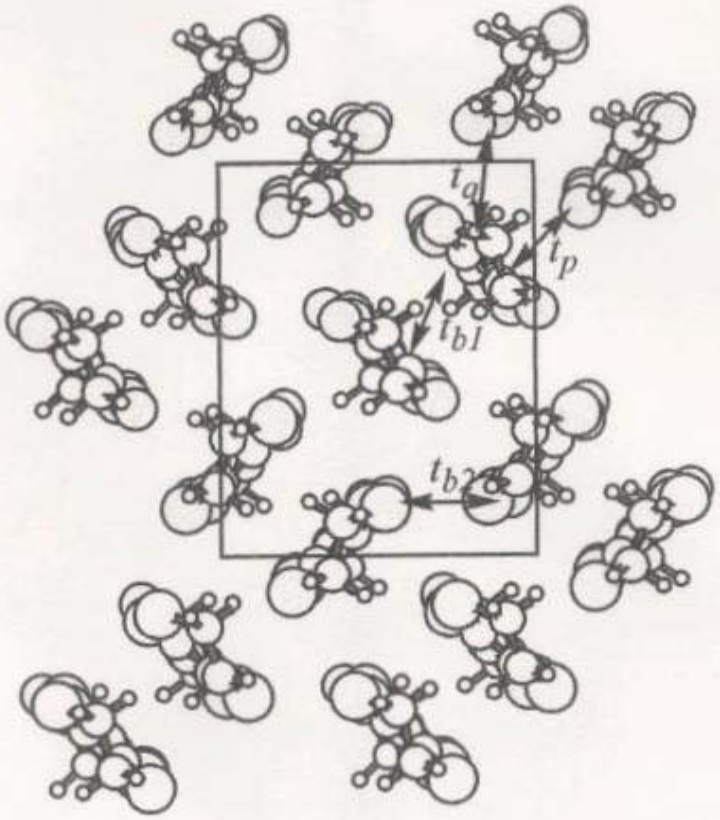

Fig. 1.5. The structure of the κ-phase BEDT-TTF conducting layer and definitions of transfer integrals.

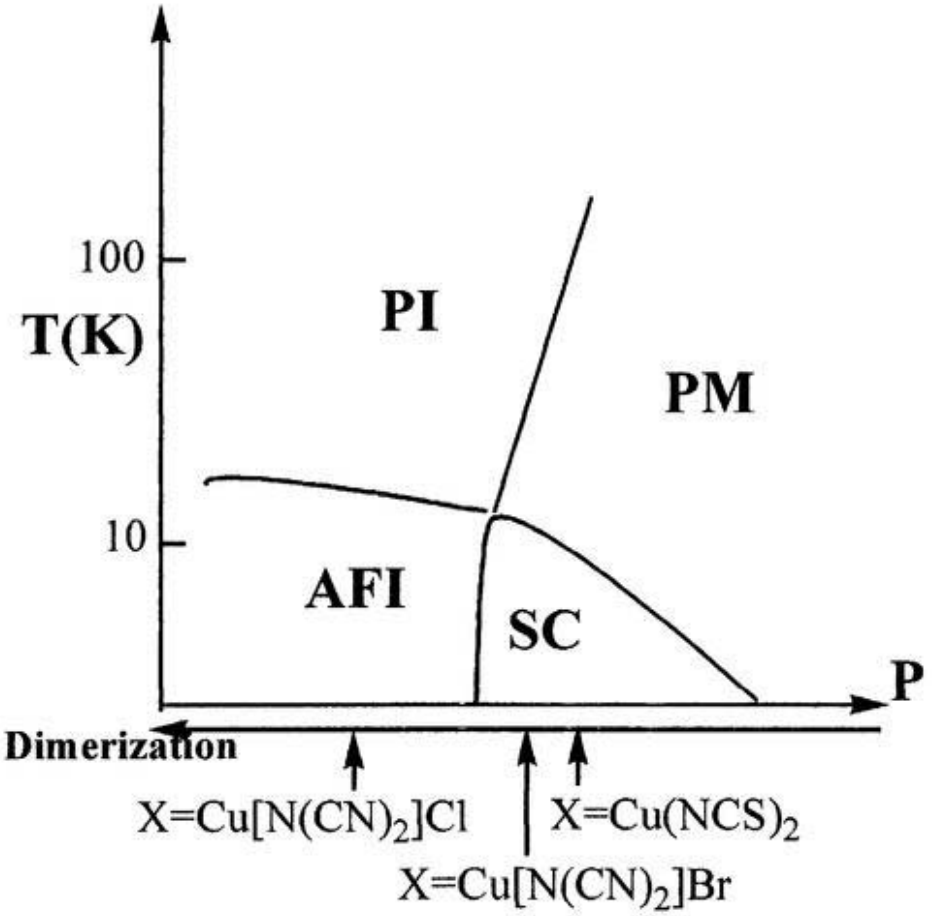

Fig. 1.6. An experimental phase diagram of κ-(BEDT-TTF)$_2$X as a function of pressure (P) and temperature (T). Here, PM, AFI, PI and SC denote paramagnetic metal, antiferromagnetic insulator, paramagnetic insulator, and superconductor, respectively.

Reference

[1] L. B. Coleman, M. J. Cohen, D. J. Sandman, F. F. Yamagishi, A. F. Garito, and A. J. Heeger, Solid State Commun. 12, 1125 (1973).

[2] S. Kagoshima, H. Anzai, K. Kajimura, and T. Ishiguro, J. Phys. Soc. Jpn. 39, 1143 (1975).

[3] D. Jerome, A. Mazaud, M. Rimbault and K. Bechgaard, J. Phys. Lett. 41, L95 (1980).

[4] D. Jerome, Organic Conductors, ed. J. -P. Farges, Marcel Dekker, N.Y., 1994.

[5] R. Kato, Y. -L. Liu, Y. Hosokoshi and S. Aonuma, Mol. Cryst. Liq. Cryst. 296, 217 (1997).

[6] A. Aumüller, P. Erk, G. Klebe, S. Hünig, J. U. von Schütz, and H. –P. Werner, Angew. Chem. Int. Ed. Engl. 25, 740 (1986).

[7] K. Sinzger, S. Hünig, M. Jopp, D. Bauer, W. Bietsch, J. U. von Schütz, H. C. Wolf, R. K. Kremer, T. Metzenthin, R. Bau, S. I. Khan, A. Lindbaum, C. L. Lengauer and E. Tillmanns, J. Am. Chem. Soc. 115, 7696 (1993).

[8] R. Kato, H. Kobayashi and A. Kobayashi, J. Am. Chem. Soc. 111, 5224 (1989)

[9] R. Moret, Synth. Met. 27, B301 (1998).

[10] A. Kobayashi, R. Kato, H. Kobayashi, T. Mori and H. Inokuchi, Solid State Commun. 45, 64 (1987).

[11] K. Hiraki and K. Kanoda, Phys. Rev. B 54, R17276 (1996).

[12] K. Hiraki, Doctoral thesis, The Graduate University for Advanced Studies (1997).

[13] R. Moret, P. Erk, S. Hünig and J. U. Von Shültz, J. Phys. 49, 1925 (1998).

[14] R. Kato, S. Aonuma and H. Sawa, Mol. Cryst. Liq. Cryst. 284, 183 (1996).

[15] H. Seo and H. Fukuyama, J. Phys. Soc. Jpn. 66, 1249 (1997).

[16] N. Kobayashi and M. Ogata, J. Phys. Soc. Jpn. 66, 3356 (1997).

[17] N. Kobayashi, M. Ogata and K. Yonemitsu, J. Phys. Soc. Jpn. 67, 1098 (1998).

[18] Y. Suzumura and H. Fukuyama, J. Phys. Soc. Jpn. 61, 3322 (1992).

[19] T. Ogawa and Y. Suzumura, J. Phys. Soc. Jpn. 63, 1494 (1994).

[20] T. Ogawa and Y. Suzumura, J. Phys. Soc. Jpn. 63, 2066 (1994).

[21] T. Ogawa and Y. Suzumura, Phys. Rev. B 51, 10293 (1995).

[22] T. Ogawa and Y. Suzumura, Phys. Rev. B 53, 7085 (1996).

[23] S. Suzuki, T. Ogawa, and Y. Suzumura, J. Phys. Soc. Jpn. 65, 2577 (1996).

[24] T. Ogawa and Y. Suzumura, J. Phys. Soc. Jpn. 66, 690 (1997).

[25] T. Miyazaki, K. Terakura, Y. Morikawa and T. Yamasaki, Phys. Rev. Lett. 74, 5104 (1995).

[26] T. Miyazaki and K. Terakura, Phys. Rev. B 54, 10452 (1996).

[27] T. Miyazaki and K. Terakura, Phys. Rev. B 56, R477 (1997).

[28] K. Yonemitsu, Phys. Rev. B 56, 7262 (1997).

[29] H. H. Wang, K. D. Carlson, U. Geiser, A. M. Kini, A. J. Schultz, J. M. Williams, L. K. Montgomery, W. K. Kwok, U. Welp, K. G. Vandervoort, S. J. Boryschuk, A. V. Strieby Crouch, J. M. Kommers, D. M. Watkins, J. E. Schirber, D. L. Overmyer, D. Jung, J. J. Novoa, and M. -H. Whangbo, Synth. Met. 42, 1983 (1991).

[30] U. Geiser, A. J. Schultz, H. H. Wang, D. M. Watkins, D. L. Stupka, J. M. Williams, J. E. Schirber, D. L. Overmyer, D. Jung, J. J. Novoa and M. -H. Whangbo, Physica C 174, 475 (1991).

[31] Y. -N. Xu, W. Y. Ching, Y. C. Jean and Y. Lou, Phys. Rev. B 52, 12946 (1995).

[32] E. Demiralp and W. A. Goddard III, J. Phys. Chem. 98, 9781 (1994).

[33] E. Demiralp, S. Dasgupta, and W. A. Goddard III, J. Am. Chem. Soc. 117, 8154 (1995).

[34] E. Demiralp, S. Dasgupta, and W. A. Goddard III, J. Phys. Chem. A 101, 1975 (1997).

[35] E. Demiralp and W. A. Goddard III, Phys. Rev. B 56, 11907 (1997).

[36] E. Demiralp and W. A. Goddard III, J. Phys. Chem. A 102, 2466 (1998).

[37] H. Kino and H. Fukuyama, J. Phys. Soc. Jpn. 64, 1877 (1995).

[38] H. Kino and H. Fukuyama, J. Phys. Soc. Jpn. 64, 2726 (1995).

[39] H. Kino and H. Fukuyama, J. Phys. Soc. Jpn. 64, 4523 (1995).

[40] A. Fortunelli and A. Painelli, J. Chem. Phys. 106, 8041 (1997).

[41] A. Fortunelli and A. Painelli, J. Chem. Phys. 106, 8051 (1997).

[42] A. Fortunelli and A. Painelli, Phys. Rev. B 55, 16088 (1997).

[43] G. Visentini, A. Painelli, A. Girlando, and A. Fortunelli, Europhys. Lett. 42, 467 (1998).

[44] Y. Okuno and H. Fukutome Solid State Commun. 101, 355 (1997).

[45] C. E. Campos and P. S. Sandhu, J. S. Brooks and T. Ziman, Phys. Rev. B 53, 12725 (1996).

[46] M. Gusmao and T. Ziman, Phys. Rev. B 54, 16663 (1996).

[47] H. Kino and H. Kontani, J. Phys. Soc. Jpn. 67, 3691 (1998).

[48] H. Kondo and T. Moriya, J. Phys. Soc. Jpn. 67, 3695 (1998).

[49] J. Schmalian, Phys. Rev. Lett. 81, 4232 (1998).

Chapter 2.

Theoretical Treatment of Organic Conductors

Ab Initio MO Studies on Electronic States of DCNQI Molecules
Y. Imamura, S. Ten-no, Y. Tanimura
J. Phys. Chem. B 103, 266 (1999).

Theoretical study on electron correlation of 1-D$(DCNQI)_2M$ (M=Li, Ag) salts
Y. Imamura, S. Ten-no, K. Yonemitsu, Y. Tanimura
Chem. Phys. Lett. 298, 15 (1998).

We explain the computational details of structural monomer optimization and oligomer calculations by the ab initio MO method and describe the way to evaluate transfer integrals and Coulomb interactions for the DCNQI salts in chapter 2.1.1. Those of the κ-BEDT-TTF salts are also given in chapter 2.1.2. The Construction of effective Hamiltonian and exact diagonalization method for the DCNQI and κ-BEDT-TTF salts are described in chapter 2.2.1 and 2.2.2, respectively. We explain the results of the 2-D extended Hubbard model within the HF approximation in chapter 2.3.1.

2.1 Ab initio HF calculation and parametrization of effective Hamiltonian

2.1.1 $(DCNQI)_2M$ salts

Structures of anionic and neutral DCNQI monomers are optimized at HF level with several Gaussian-type basis sets and compared with experimental data. We assume that R1,R2-DCNQI molecules (R1=R2) are of Ci symmetry and have planar structures except the substituents, R1 and R2. Three different basis sets, the single-zeta (SZ) [1], valence double-zeta (DZ) [2-4] and DZ plus polarization (DZP) [2-4] sets are used for comparisons. Those kinds of basis sets are explained in the appendix of this chapter in detail.

In this study, we perform the oligomer calculations using ab initio MO method to construct the effective Hamiltonian, H_{eff}. In order to obtain the parameters of H_{eff} such as transfer integrals, we calculate the electronic structures of stacked DCNQI dimers with various formal charges (q_d) = 0~−4 for M= Cu. A DCNQI trimer with q_d = −2 is also calculated to check the size dependence of cluster. For M= Ag, Li, a DCNQI tetramer is calculated to construct effective Hamiltonian with q_d = 0, −2. In the oligomer calculations, we use structural parameters from the X-ray diffraction (XRD)

experiments at various temperatures [5-9]. In this study, we consider temperature effects as the changes of structural parameters. We also adopt the SZ, DZ and DZP basis sets for the DCNQI dimer calculation. For the DCNQI trimer, the Stevens-Basch-Krauss-Jasien (SBK) split valence plus polarization basis sets and their effective core potentials (ECP) (SBK-31G*) [10] are used. For DCNQI tetramer, SBK-31G is adopted.

We define two types of transfer integrals based on DCNQI dimer calculations with $q_d = -1$. Henceforward, we use the spatial orbital indices, $i, j, \ldots$, $s, t, \ldots$, $\lambda, \ldots$ and $p, q, \ldots$ for the doubly occupied, singly occupied (SOMO), localized (LMO) and general molecular orbitals, respectively. A transfer integral, $t(1)$, can be defined by the half of the energy difference between the ^2A_g ground and ^2A_u first excited states, i.e.,

$$t(1) = \frac{1}{2}\left[E(^2A_g) - E(^2A_u)\right]. \tag{2.1}$$

We perform the restricted open shell HF (ROHF) calculations for these states whose energies are given by

$$E(S) = \langle s|f(S)|s\rangle + E_{core}(S), \tag{2.2}$$

where S means the orbitals are optimized with respect to the state, $s = a_g, a_u$ for $S = A_g, A_u$, respectively. In the ROHF calculations, we constrain that SOMOs of the ^2A_g ground and ^2A_u first excited states have a_g, a_u symmetries, respectively. f and E_{core} are defined as

$$\langle p|f|q\rangle = \langle p|h|q\rangle + \sum_i \left[2\langle ip|iq\rangle - \langle ip|qi\rangle\right], \tag{2.3}$$

$$E_{core} = \sum_i \left[\langle i|h|i\rangle + \langle i|f|i\rangle\right]. \tag{2.4}$$

Here, h represents the one-electron Hamiltonian of the dimer model and the Dirac notation is used for two-electron integrals. Another transfer integral, $t(2)$, can be defined as

$$t(2) = \langle \lambda_1 | f | \lambda_2 \rangle, \tag{2.5}$$

where λ_1 and λ_2 denote LMOs which are equivalently located on each DCNQI

molecule. As the canonical MOs and LMOs are connected via the unitary transformation,

$$|a_g\rangle = \frac{1}{\sqrt{2}}[|\lambda_1\rangle + |\lambda_2\rangle], \tag{2.6}$$

$$|a_u\rangle = \frac{1}{\sqrt{2}}[|\lambda_1\rangle - |\lambda_2\rangle], \tag{2.7}$$

it is easy to confirm that $t(1)$ is equivalent to $t(2)$ for a given set of MOs. However, in the $t(1)$, MOs are optimized separately to the two states. Thus the orbital relaxation is neglected in $t(2)$. We use the Boys' localization procedure [11] for the LMOs based on the ground state HF calculation. A similar estimation is also performed for the DCNQI trimer. Besides the transfer integrals, on-site and nearest-neighbor Coulomb interactions, $\langle\lambda_1\lambda_1|\lambda_1\lambda_1\rangle$ and $\langle\lambda_1\lambda_2|\lambda_1\lambda_2\rangle$, are estimated by using the same LMOs. All calculations are performed by the GAMESS [12] and GAUSSIAN [13] suites of program packages.

2.1.2 $(BEDT\text{-}TTF)_2Cu[N(CN)_2]X$ salts (X= Cl, Br and I)

In Fig. 1.4, we show two stable conformations of the BEDT-TTF molecule, i.e., the staggered and eclipsed ones. As discussed by Demiralp and Goddard, the eclipsed one is slightly lower in energy and is chosen for ab initio calculations throughout this thesis. We optimize the geometrical structure of BEDT-TTF at HF/DZP [2] with a set of coupling coefficients for the formal charge, q = +1/2 [14].

A model Hamiltonian is constructed on the basis of calculations of BEDT-TTF clusters, the dimer and a few tetramers. In all the cluster calculations, the basis set is 31G valence function with the SBK effective core potential (SBK-31G). In the dimer calculations, the original basis functions are augmented by d-polarization functions for non-hydrogen atoms (SBK-31G*). The formal charges are +1, and 0, +2 for the dimer and tetramers, respectively. We freeze all atoms except hydrogen atoms at the locations determined by the XRD experiment [15] and optimize the locations of hydrogen atoms in the dimer unit at HF/SBK-31G.

To construct the model Hamiltonian, we obtain highest ocuupied molecular orbitals (HOMO) 1-2 for the dimer and HOMO1-4 for the tetramers and localize them on each BEDT-TTF molecule following the Boys localization procedure. Here, HOMO is spatial orbitals referred to neutral species. We evaluate transfer integrals in two different manners, $t(1)$ and $t(2)$, based on the dimer calculation. The spatial orbital indices are defined in chapter 2.1.1. The transfer integral, $t(1)$, is a half of the energy difference between the ground and first excited states, i.e., ${}^2A_u$ and ${}^2A_g$ in the Ci frame. This estimation is the same as for the DCNQI salts.

The transfer integral, $t(2)$, is defined as

$$t(2) = \langle \lambda_1 | \tilde{f} | \lambda_2 \rangle, \tag{2.8}$$

where λ_1 and λ_2 are LMOs located on the first and second BEDT-TTF molecules and the operator $\tilde{f}$ is given by

$$\langle p | \tilde{f} | q \rangle = \langle p | h | q \rangle + \sum_{i \neq HOMO1-2} \left[2\langle ip | iq \rangle - \langle ip | qi \rangle \right], \tag{2.9}$$

where two electron integrals including HOMO1-2 are not considered because these two electron integrals are considered for exact diagonalization calculation (Full-configuration interaction (CI)). In BEDT-TTF tetramer calculations, we also estimate $t(2)$ using a similar procedure.

On-site and nearest-neighbor Coulomb interactions are estimated in BEDT-TTF dimer calculations at HF/SBK+31G*. The other long-range Coulomb interactions are estimated in BEDT-TTF tetramer calculations at HF/SBK-31G. We used the same program packages as in chapter 2.1.1.

2.2 Effective Hamiltonian and exact diagonalization

2.2.1 DCNQI-Ag, Li salts

Henceforward, the spatial orbital indices, $p,q,\ldots$ are used for the LMOs. For the effective Hamiltonian over LMOs,

$$H_{eff} = \sum_{pq} \langle p \mid h \mid q \rangle E_{pq} + \frac{1}{2} \sum_{pqrs} \langle pq \mid rs \rangle (E_{pr} E_{qs} - \delta_{qr} E_{ps}), \tag{2.10}$$

where $E_{pq} = a_{p\uparrow}^{+} a_{q\uparrow} + a_{p\downarrow}^{+} a_{q\downarrow}$. For DCNQI-M (M=Li, Ag) salts, we construct two different effective Hamiltonians, $H_{eff}(1)$ and $H_{eff}(2)$. In $H_{eff}(1)$, the one-electron part consists of diagonal and off-diagonal elements over the nearest-neighbor LMOs, and the two-electron part is of the four type integrals, $\langle pp|pp\rangle$, $\langle pq|pq\rangle$, $\langle pq|qp\rangle$ and $\langle pp|pq\rangle$ where p and q represent the nearest-neighbor LMOs. In $H_{eff}(2)$, the one-electron part includes diagonal elements and off-diagonal elements over LMOs up to the third nearest-neighbor orbitals, and the two-electron one includes transformed two-electron integrals up to the third-nearest-neighbor orbitals. In $H_{eff}(1)$ and $H_{eff}(2)$, one- and two-electron integrals up to the nearest- neighbor orbitals are obtained from the middle two DCNQI LMOs of a DCNQI tetramer. In $H_{eff}(2)$, one- and two-electron integrals over LMOs of the second and third nearest-neighbor orbitals are obtained from DCNQI tetramer calculations. We take an average of multiplicated integrals which contribute to a matrix element of $H_{eff}(2)$ to maintain the translational symmetry. We employ the Slater-determinant-based direct configuration interaction (CI) method for diagonalizing the effective Hamiltonians [16]. We use the periodic and anti-periodic boundary conditions for the DCNQI tetramer and octamer models, respectively, in Fig. 2.1 so that the ground state does not become an artificial high multiplet state due to the finite-size effect. We analyze the electronic phases of the obtained states using the spin correlation function,

$$\Delta_{p\sigma,q\sigma'} = \langle n_{p\sigma} n_{q\sigma'} \rangle / N^2, \tag{2.11}$$

where $n_{p\sigma} = a_{p\sigma}^{+} a_{p\sigma}$ and $N = \langle n_{p\sigma} \rangle$.

2.2.2 κ–(BEDT-TTF)$_2$Cu[N(CN)$_2$]X salts (X= Cl, Br and I)

There are three electrons per dimer so that the upper molecular orbital (UMO) is half-filled. Therefore the electronic properties mainly depend on the UMOs. To elucidate the effect of electron correlation, we employ an effective Hamilitonian over the UMOs

$$H_{eff} = \sum_{\substack{m,n(m\neq n)\\ \sigma}} t_{mn} a^{+}_{m\sigma} a_{n\sigma} + \sum_{m} \langle mm \mid mm \rangle n_{m\uparrow} n_{m\downarrow} + \frac{1}{2} \sum_{m,n(m\neq n)} \langle mn \mid mn \rangle n_m n_n , \qquad (2.12)$$

where the indices, m,n...., and σ, denote UMOs and spins, $n_{p\sigma} = a^{+}_{p\sigma} a_{p\sigma}$ and $n_p = a^{+}_{p\uparrow} a_{p\uparrow} + a^{+}_{p\downarrow} a_{p\downarrow}$. The UMO $|m\rangle$ is defined by

$$|m\rangle = \frac{1}{\sqrt{2}} \left[|\lambda_1\rangle - |\lambda_2\rangle \right] , \qquad (2.13)$$

where both of λ_{1-2} belong to one and the same dimer. One- and two-electron interactions over UMOs are calculated by transforming the HF integrals of the κ-(BEDT-TTF)$_2$Cu[N(CN)$_2$]Br salt at 127 K. In this particular work, we use two different model Hamiltonians, $H_{eff}(1)$ and $H_{eff}(2)$. These Hamiltonians include the same one-electron interactions and include the two-electron interactions up to the nearest-neighbor and next-nearest-neighbor dimers, respectively. The off-diagonal one-electron interaction is estimated from the half of the energy difference between the first and second HOMO orbital energies in the tetramer calculation. We use the periodic boundary condition for the decamer model shown in Fig. 2.2 and analyze the electronic phases of the obtained states using the spin correlation function.

2.3 Model Hamiltonian and HF approximation

2.3.1 κ–(BEDT-TTF)$_2$Cu[N(CN)$_2$]X salts (X= Cl, Br and I)

To clarify the effects of the long-range Coulomb interactions in κ-BEDT-TTF salts, we introduce a 2-D extended Hubbard model by extracting their 2-D conducting plane and neglecting their anion layers. The indices, $i, j, \ldots$, denote HOMOs localized on the BEDT-TTF molecules. The Hamiltonian is defined by

$$H = \sum_{i,j,\sigma} t_{ij} a_{i\sigma}^{+} a_{j\sigma} + \sum_{i} U n_{i\uparrow} n_{i\downarrow} + \sum_{i \neq j} V_{ij} n_i n_j, \tag{2.14}$$

where t_{ij}, V_{ij}, and U denote transfer integral and Coulomb interaction between i and j sites, and on-site Coulomb interaction, respectively. We include Coulomb interaction, V_{ij}, up to the next-nearest-neighbor dimer as shown in Fig. 2.3. The Coulomb interactions, V_{13} and V_{27}, are referred to as V_{NN} and V_{NNN}, respectively. The unit cell includes four BEDT-TTF molecules, that is, two dimers as shown in Fig. 1.5. We fix the ratios among the nearest-neighbor interactions, *i.e.*, V_{15}/V_{13}, V_{14}/V_{13} and V_{16}/V_{13} and the ones among the next-nearest-neighbor interactions, *i.e.*, V_{29}/V_{27}, V_{210}/V_{27}, V_{17}/V_{27}, V_{18}/V_{27} and V_{110}/V_{27} to elucidate the physical properties, regarding the BEDT-TTF dimer as a unit. The densities are determined self-consistently and the electron occupation is fixed to be 6 electrons in 4 molecules.

We apply the HF approximation,

$$U n_{i\uparrow} n_{i\downarrow} \approx U(\langle n_{i\uparrow} \rangle n_{i\downarrow} + n_{i\uparrow} \langle n_{i\downarrow} \rangle - \langle n_{i\uparrow} \rangle \langle n_{i\downarrow} \rangle), \tag{2.15}$$

$$\begin{aligned} V_{ij} n_i n_j \approx V_{ij} (&\langle n_i \rangle n_j + n_i \langle n_j \rangle - \langle n_i \rangle \langle n_j \rangle - \langle a_{i\uparrow}^{+} a_{j\uparrow} \rangle a_{j\uparrow}^{+} a_{i\uparrow} - a_{i\uparrow}^{+} a_{j\uparrow} \langle a_{j\uparrow}^{+} a_{i\uparrow} \rangle \\ &+ \langle a_{i\uparrow}^{+} a_{j\uparrow} \rangle \langle a_{j\uparrow}^{+} a_{i\uparrow} \rangle - \langle a_{i\downarrow}^{+} a_{j\downarrow} \rangle a_{j\downarrow}^{+} a_{i\downarrow} - a_{i\downarrow}^{+} a_{j\downarrow} \langle a_{j\downarrow}^{+} a_{i\downarrow} \rangle + \langle a_{i\downarrow}^{+} a_{j\downarrow} \rangle \langle a_{j\downarrow}^{+} a_{i\downarrow} \rangle). \end{aligned} \tag{2.16}$$

The ground state of the Hamiltonian is calculated using 20×30 k-points on the $a^* \times c^*$ conducting plane in the momentum space. The electron densities are given by

$$n_{i\sigma} = \frac{1}{N_{cell}} \sum_{a}^{occ} \sum_{k} c_{kai\sigma}^{*} c_{kai\sigma}, \tag{2.17}$$

where N_{cell} represents the total number of cells and the coefficient of the a'th eigenvector of i'th site at k point in the Brillouin zone is written as $c_{kai\sigma}$.

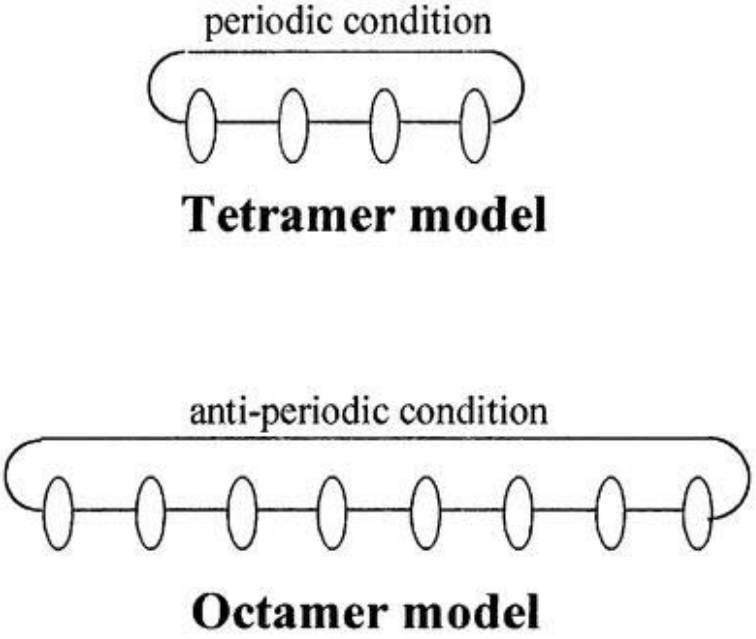

Fig. 2.1. DCNQI tetramer and octamer models

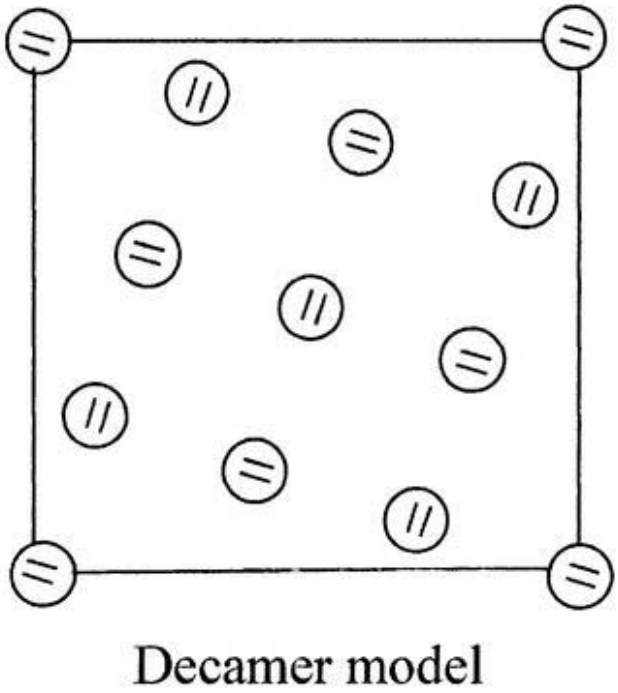

Fig. 2.2. BEDT-TTF decamer model

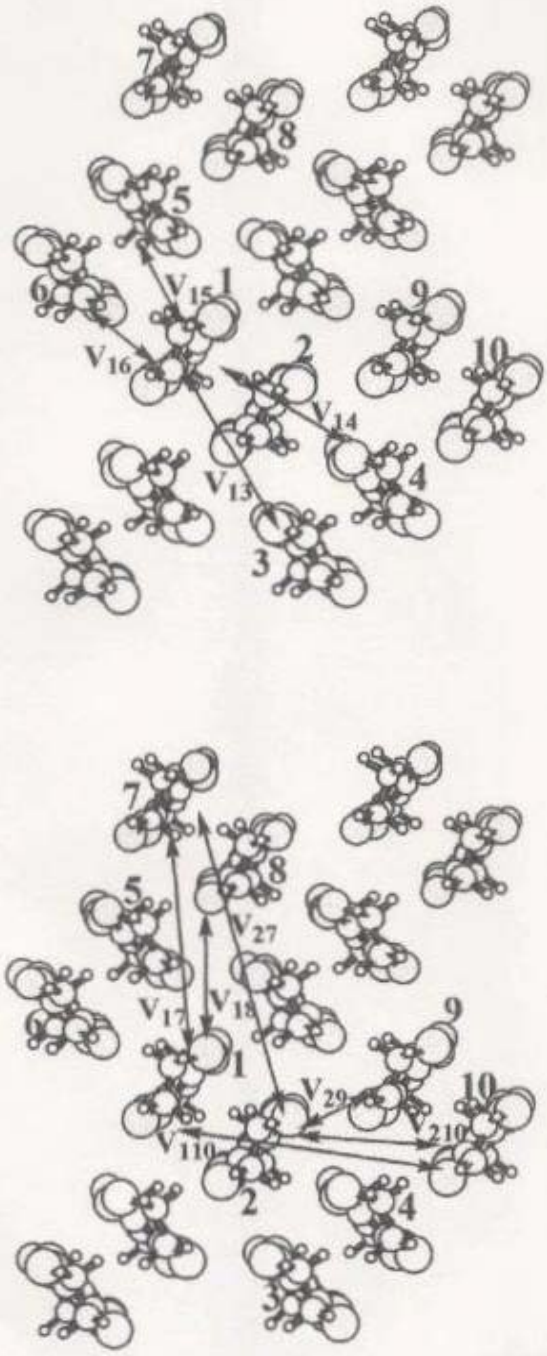

Fig. 2.3. Nearest-neighbor Coulomb interactions (top) and next-nearest-neighbor Coulomb interactions (bottom).

Appendix Basis sets

Representative basis functions are two kinds of functions, Slater and Gauss type functions. Slater type function is given by,

$$\left(\frac{\zeta^3}{\pi}\right)^{1/2} e^{-\zeta r}$$

On the other hand, Gauss type function is given by,

$$\left(\frac{\alpha^3}{\pi}\right)^{1/2} e^{-\alpha r^2}$$

The character of Slater function is appropriate for describing the electronic wave function. However, Gauss functions (GF) are widely used because it is easy to calculate two electron integrals.

Linear combination of primitive Gauss functions are used for basis set to reduce the amount of calculation,

$$\phi_\mu^{CGF}(r-R_A)=\sum_{p=1}^{N} d_{p\mu}\phi_p^{GF}(\alpha_{p\mu},\mathbf{r}-\mathbf{R}_A)=\sum_{p=1}^{N} d_{p\mu}e^{-\alpha_{p\mu}(\mathbf{r}-\mathbf{R}_A)}$$

where μ, R_A and N represent type of orbital, center of atoms and the number of GF. This linear combination is called contraction. To fit Slater function, the best contraction coefficients, $d_{p\mu}$ and exponents $\alpha_{p\mu}$, are determined. Contracted Gauss function (CGF) often used is STO-NG where a linear combination of N Gauss functions is fitted to Slater function. Generally, STO-NG, contracted N Gauss functions, is called minimal basis sets.

Split valence basis set, such as 3-21G and 6-31G, has two kinds of basis functions for each valence orbital. This basis set is called DZ basis set. For example, for 6-31G basis set, core orbitals are described by contracted 6 Gauss functions and valence orbitals are two kinds of contracted 1 and 3 Gauss functions. Similarly, the triple zeta basis sets have three kinds of basis functions.

To describe the electron population in bonding region, we add the basis functions

which is higher angular momentum for calculation. This function is called polarization function. The representative polarization basis set 6-31G(d) or 6-31G* has d functions added into heavy atoms. The basis set 6-31G(d,p) or 6-31G** has not only d functions added into heavy atoms but also p function added to hydrogen. The double zeta and polarization basis set is often called DZP or DZ + P.

Reference

[1] S. Huzinaga, J. Andzelm, M. Klobukowski, E. Radzio-Andzelm, Y. Sakai and H. Tatewaki, Gaussian Basis Sets for Molecular Calculations, Elsevier, Amsterdam, 1984.

[2] T. H. Jr. Dunnig and P. J. Hay, Method of electronic structure theory, ed. H. F. Schaefer III, Plenum Press, N. Y., 1977.

[3] R. C. Jr. Binning and L. A. Curtiss, J. Comp. Chem. 11, 1206 (1990).

[4] K. D. Dobbs and W. J. Hehre, J. Comp. Chem. 7, 359 (1986).

[5] K. Sinzger, S. Hünig, M. Jopp, D. Bauer, W. Bietsch, J. U. von Schütz, H. C. Wolf, R. K. Kremer, T. Metzenthin, R. Bau, S. I. Khan, A. Lindbaum, C. L. Lengauer and E. Tillmanns, J. Am. Chem. Soc. 115, 7696 (1993).

[6] R. Kato, H. Kobayashi and A. Kobayashi, J. Am. Chem. Soc. 111, 5224 (1989).

[7] H. Sawa (private communication)

[8] A. Kobayashi (private communication)

[9] K. Hiraki, Doctoral thesis, The Graduate University for Advanced Studies (1997).

[10] W. J. Stevens, H. Basch and M. J. Krauss, J. Chem. Phys. 81, 6026 (1984).

[11] S. F. Boys, Quantum Science of Atoms, Molecules, and Solids, ed. P. O. Lowdin, Academic press, N. Y., 1966.

[12] M. W. Schmidt, K. K. Baldridge, J. A. Boatz, S. T. Elbert, M. S. Gordon, J. H. Jensen, S. Koseki, N. Matsunaga, K. A. Nguyen, S. J. Su, T. L. Windus, M. Dupuis, and J. A. Montgomery, J. Comp. Chem. 14, 1347 (1993).

[13] M. J. Frisch, G. W. Trucks, H. B. Schlegel, P. M. W. Gill, B. G. Johnson, M. A. Robb, J. R. Cheeseman, T. A. Keith, G. A. Petersson, J. A. Montgomery, K. Raghavachari, M. A. Al-Laham, V. G. Zakrzewski, J. V. Ortiz, J. B. Foresman, C. Y. Peng, P. Y. Ayala, M. W. Wong, J. L. Andres, E. S. Replogle, R. Gomperts, R. L. Martin, D. J. Fox, J. S. Binkley, D. J. Defrees, J. Baker, J. P. Stewart, M. Head-

Gordon, C. Gonzalez, and J. A. Pople, Gaussian 94, Gaussian, Inc., Pittsburgh PA, 1995.

[14] The used coupling coefficients were $f_1 = 1$, $f_2 = 0.75$, $\alpha_{11} = 2$, $\alpha_{12} = 1.5$, $\alpha_{22} = 0.5$, $\beta_{11} = -1$, $\beta_{12} = -0.75$, $\beta_{22} = 0$ in the energy expression,

$$E = 2\sum_j f_i h_{ii} + \sum_{i,j} \alpha_{ij} \langle ij|ij\rangle + \beta_{ij} \langle ij|ji\rangle,$$

where the indices, 1 and 2, denote doubly occupied and 3/4 filled orbitals, respectively.

[15] U. Geiser, A. J. Schultz, H. H. Wang, D. M. Watkins, D. L. Stupka, J. M. Williams, J. E. Schirber, D. L. Overmyer, D. Jung, J. J. Novoa and M. -H. Whangbo, Physica C 174, 475 (1991).

[16] P. J. Knowles and N. C. Handy, Chem. Phys. Lett. 111, 315 (1984).

Chapter 3.

Geometrical and Electronic Structures of DCNQI Salts

Ab Initio MO Studies on Electronic States of DCNQI Molecules
Y. Imamura, S. Ten-no, Y. Tanimura
J. Phys. Chem. B 103, 266 (1999).

Theoretical study on electron correlation of 1-D$(DCNQI)_2M$ (M=Li, Ag) salts
Y. Imamura, S. Ten-no, K. Yonemitsu, Y. Tanimura
Chem. Phys. Lett. 298, 15 (1998).

3.1 Geometrical structure and parameters of effective Hamiltonian

3.1.1 Molecular structure of DCNQI

Structural parameters of DCNQI monomers are optimized at HF/DZP level and are shown in Table 3.1 and structural parameters are defined in Fig. 1.1. Andreetti *et al.* studied the crystal structure consisting of DCNQI molecules with neutral charges [1]. These parameters are shown in Table 3.2. Comparing them, we can see that the errors of the bond distances and angles are within 0.04 Å and 1 degree, respectively except the parameter (h), which is about 4 degrees different from the XRD experiment. This is because crystal effects are not included in these calculations. The bond lengths (d,e) of the neutral DCNQI molecule are about 1.48 Å which is shorter than the theoretical value of ethane, 1.531 Å, obtained by the calculation at HF/DZP level. On the other hand, the bond length (f) is about 1.330 Å which is a little longer than the theoretical value of ethylene, 1.325 Å, obtained by the calculation at the same level. These results imply the resonance in the DCNQI molecules. For neutral and anionic DCNQI molecules, the bond lengths (d) of R= -Me, -OMe is longer than that of other DCNQI molecules, on the contrary, the bond length (e) is shorter. This is due to the steric effects of substituents. However, the influence of substituents on the six-membered ring structure is small. The DI-DCNQI salts show a unique phase diagram under high pressure [2]. As long as the molecular structure is concerned, however, there is no prominent difference between DI-DCNQI and other DCNQI derivatives. The unique character of DI-DCNQI salts is probably due to the crystal structure or electronic states through the crystals.

Comparing the neutral DCNQI and anionic $DCNQI^-$ structures, we found the bond lengths (c,f) of DCNQI are shorter than those of $DCNQI^-$, whereas the bond lengths (b,d,e) are longer. Especially the parameter (c) of DCNQI is about 0.06 Å longer due to the anti-bonding nature of $-C_2-N_2-$. We will discuss this point in a later section. We now compare our results with the experimental and first-principles calculation results.

DCNQI crystal structures of copper salts were studied experimentally by Sinzger *et al*, Kobayashi *et al.* and Sawa (Table 3.2) [3-5]. In the metallic state, the formal charge of Cu is close to +4/3 and that of DCNQI molecule is −2/3. In Table 3.3, we show the average structural parameters of $DCNQI^{-2/3}$ derived from those of neutral DCNQI and anionic $DCNQI^{-}$. The errors of bond distances and angles between experimental and theoretical structures are within 0.04 Å and 5 degrees, respectively. The errors of the angles are large because we neglect the Cu coordinated by cyano groups at the end of the DCNQI molecule. We should stress, however, that the structural parameters we obtained are in good agreement with the experimental ones.

We then compare our results with those from first-principles calculations based on the DFT [6]. The largest discrepancies in bond lengths and angles are 0.03 Å and 0.7 degrees, respectively. Most of the bond lengths are reproduced within errors of 0.01 Å.

In Table 3.4, we show the basis set dependence of the structural parameters. Large errors of bond lengths are clearly seen in the SZ basis set case. The structural parameters of the DZP basis set is similar to those of DZ one, but some improvements are found in the bond lengths of double and triple bonds and in the angle of $-N_2-C_1-N_1$.

3.1.2 HOMO and LUMO

The HOMO and LUMO of the DCNQI molecule are drawn in Fig. 3.1. The anti-bonding characters of $-N_2-C_2-$ and $-C_3-C_4-$ are observed in LUMO. As seen in the previous section, these bond lengths of anionic $DCNQI^{-}$ molecules are longer than those of neutral one. The LUMO coefficients of p-type orbitals in $-N_2-$ and the six-membered ring are large but those of the substituent are small. This indicates that the six-membered ring and $-N_2-C_1-N_1$ play an important role in the conductivity of DCNQI crystals.

3.1.3 Parameters of effective Hamiltonian of DCNQI-Cu salts

We calculate DCNQI dimers of different formal charges, q_d =0-4 using the

structural parameters obtained from the XRD experiments. The parameters obtained by those calculations are shown in Table 3.5. We could not obtain *t(1)* except DMe-DCNQI at room temperature and DI-DCNQI at 9K because of poor convergence. On-site and nearest-neighbor Coulomb interactions change scarcely by the formal charges. *t(2)* is similar for $q_d = 0, -1$ and -2 but are different with $q_d = -3$ and -4. These differences are explained by the separation of LMOs because there is strong electron repulsion due to extra minus charges in finite cluster. We choose $q_d = -1$ for DCNQI dimer which is close to that of Cu-DCNQI dimer, $-4/3$. For DMe-DCNQI dimer at room temperature, *t(1)* is calculated as 0.356 eV which is slightly smaller than the corresponding *t(2)*, 0.380 eV. This difference is mostly explained by the orbital relaxation because the HF orbitals are optimized under the symmetry Ag and Au, respectively. For DMe-DCNQI dimer at room temperature, on-site and nearest-neighbor Coulomb interactions are calculated as 6.55 and 3.32 eV. The sign of transfer integral depends on taking phases of wave function. The absolute value of intrachain *t(2)* is calculated as 0.43 eV for DMe-DCNQI at 20K. This is larger than that of 0.25 eV calculated from DFT for (DMe-DCNQI)$_2$Cu [7]. Two reasons which are related with each other are conceivable to this discrepancy. (1) Pure model Hamiltonian parameters of DCNQI molecules are extracted in this particular work, however, the hybridization with *d*-orbitals in the Cu atoms probably requires the multiple band treatment in bulk calculations. (2) The tight-binding approximation used in analyzing the first-principles results may include ambiguity in their fitting band descriptions. The transfer integral, *t(2)* of the DI-DCNQI dimer at room temperature is smaller than those of the other dimers. This is because the lattice parameter of the c axis of the DI-DCNQI crystal is longest among calculated DCNQI salts. Based on the discussions on HOMO and LUMO, this indicates that the substituents mostly control the lattice parameters which dominate *t(2)*. This correlation is clearly seen in Fig. 3.2. Therefore, as the lattice parameters of the c axis become longer, *t(2)* increases.

We check the basis set dependence by using the SZ, DZ and DZP sets. The *t(2)*

calculated with SZ basis set is found to be small but they are similar to each other between DZ and DZP basis sets. We calculate the DMe-DCNQI salts with parameters at three different temperatures. These calculations indicate that the *t(2)* becomes large as temperature decreases. We obtain a similar tendency in the DI-DCNQI salts. To check the accuracy of the obtained *t(2)* with respect to the size of clusters, we perform trimer calculation of the DMe-DCNQI with experimental structural parameters at 100K with the ECP basis. A preliminary calculation of the dimer suggests that the ECP reproduces the *t(2)* with DZP set accurately, as shown in Table 3.5. We obtain 0.416 eV based on the trimer calculation which is slightly smaller that of the dimer calculation.

3.1.4 Parameters of Effective Hamiltonian of DCNQI-Ag/Li salts

We calculate DCNQI tetramers using the structural parameters of DCNQI-Ag/Li salts with different formal charges, q_d= 0 and −2. The calculated parameters are shown in Table 3.6 On-site and nearest-neighbor Coulomb interactions are obtained from the middle two DCNQI LMOs of the DCNQI tetramer. We obtain one on-site Coulomb interaction by the symmetry, Ci of DCNQI tetramer. For $(DMe\text{-}DCNQI)_2Ag$ salt at room temperature, on-site and nearest-neighbor Coulomb interactions with $q_d = -2$ are 6.23 eV and 3.28 eV, respectively. Those parameters are scarcely changed by the formal charge. The *t(2)* of $(DMe\text{-}DCNQI)_2Ag$ is 0.370 eV with $q_d = -2$ which is larger than the previous one, −0.22 eV calculated from the DFT [7]. Reasons are discussed above. On the other hand, for $(DI\text{-}DCNQI)_2Li$, *t(2)* are 0.274 eV and 0.226 eV with $q_d = 0$ and −2, respectively. This difference in *t(2)* for R1=R2=Me and R1=R2=I affects dimensionality which is determined by the ratio of the intracolumn to intercolumn interactions. Therefore it may be the cause of different physical properties as explained in chapter 1. Large transfer integrals enhance the screenings of Coulomb interactions. Therefore the difference in *t(2)* of DMe- and DI-DCNQI salts may also affect their correlations of charge ordering. We find for $(DMe\text{-}DCNQI)_2Ag/Li$ salts, the formal charge dependence on *t(2)* is small, whereas, for $(DI\text{-}DCNQI)_2Li$, it is large.

3.2 Electron correlation

3.2.1 Exact diagonalization study of 1-D DCNQI salts in tetramer model

We perform ab initio full-CI (exact diagonalization) calculation for finite tetramer model under the open boundary condition. For the singlet ground state, the up spin in 1 site and down spins in 3 and 4 sites (the up spin in 2 site and down spins in 3 and 4 sites) are correlated as shown in Fig. 3.3. The first singlet excited state has the AF correlation. For the triplet state, the up spins in 1 and 3 sites (2 and 4) are correlated. The population of 1 and 4 sites is larger than that of other sites due to electron repulsion. In order to avoid the effect of finite cluster, we will use periodic condition or anti-periodic conditions below.

3.2.2 Exact diagonalization study of 1-D DCNQI salts in tetramer and octamer models under the periodic and anti-periodic conditions

We study electron correlation of the H_{eff} extracted from transformed LMO integrals of $(DMe\text{-}DCNQI)_2Ag$ salt with $q_d = -2$. For the H_{eff} (1) of the tetramer model, the ground and first singlet excited states have the AF and charge ordering correlations between the first and third sites as shown in Fig. 3.4. The spin correlation function, $\Delta_{1\uparrow,3\downarrow}$ is 3.65 and $\Delta_{p\sigma,q\sigma'}$ between other sites are less than 0.02. This state corresponds to the 2 k_F SDW and 4 k_F CDW states. For the second singlet excited state, the up spin in the second site and down spin in the third site are correlated as shown in Fig. 3.4. This state corresponds to the $2k_F$ SDW and $2k_F$ CDW states. For the triplet state, the up spin in the first and third sites are correlated.

To investigate the long-range effects of Coulomb interactions, we extend the model to the octamer. For the H_{eff} (2) of the octamer model, the ground state also has the AF and charge ordering correlations in Fig. 3.5. The spin correlation function, $\Delta_{1\uparrow,3\downarrow}$ ($\Delta_{1\uparrow,7\downarrow}$), $\Delta_{1\uparrow,5\uparrow}$ and $\Delta_{1\uparrow,5\downarrow}$ are 2.75, 2.27 and 1.15. $\Delta_{1\uparrow,q\sigma'}$ (q= 2, 4, 6 and 8,

$\sigma = \uparrow$ and $\downarrow$) are less than 0.4. So, in this model, the localization is weaker than that in the tetramer model. Some low-lying excited states have similar spin-flipped CDW correlations. It is therefore elucidated that the spin correlation is weak in this octamer model. The charge ordering of these states is in good agreement with the $4k_F$ CDW state observed experimentally for the 1-D DCNQI salts [8,9].

For the tetramer and octamer models, we found that the ground state is an AF state. This state corresponds to the $4k_F$ CDW and $2k_F$ SDW states calculated by Kobayashi *et al.* and Seo and Fukuyama by the HF approximation [10-12]. In case of the tetramer model, the second singlet excited state corresponds to the $2k_F$ SDW and $2k_F$ CDW states calculated by Kobayashi *et al.* Actually, the XRD experiments of Pouget and Ravy suggested that the ground state for a similar electronic system, $(TMTSF)_2PF_6$, is the coexistence of the $2k_F$ SDW and $2k_F$ CDW states [13].

We have investigated the spin correlation based on the full-CI (exact diagonalization) calculations of the 1-D octamer and tetramer models. In these calculations, we neglect the effect of intercolumn interactions. Basically, in DCNQI-Ag/Li salts, these effects are small due to the strong 1-D character. For DI-DCNQI salt, however, intercolumn interaction is large [7] and intracolumn interaction is small in comparison with other DCNQI salts. This system has more or less 3-D character. In such a case, it may be necessary to include the intercolomn interactions in the effective Hamiltonian. The long-range behavior will be inspected more by extending the size of the model. We are proceeding this direction of research with employing the density-matrix renormarization group method to treat large-scale models.

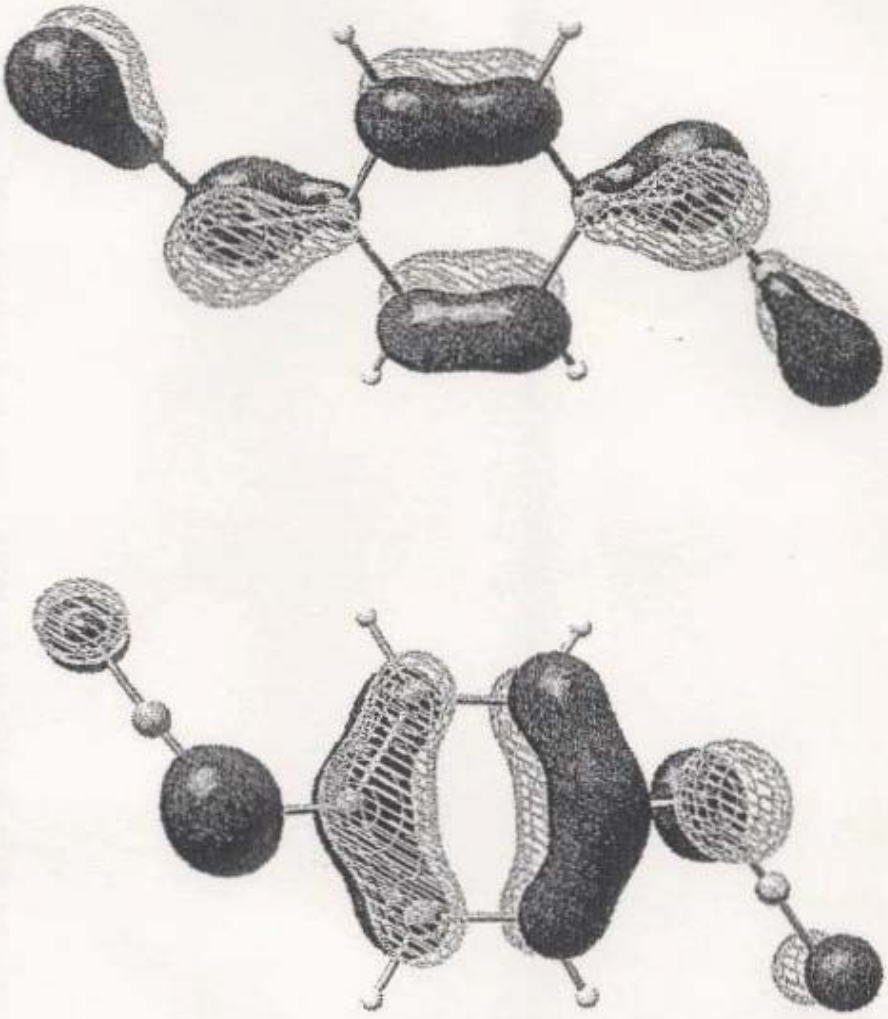

Fig. 3.1. HOMO (top) and LUMO (bottom) of neutral DCNQI molecule at HF/DZ level.

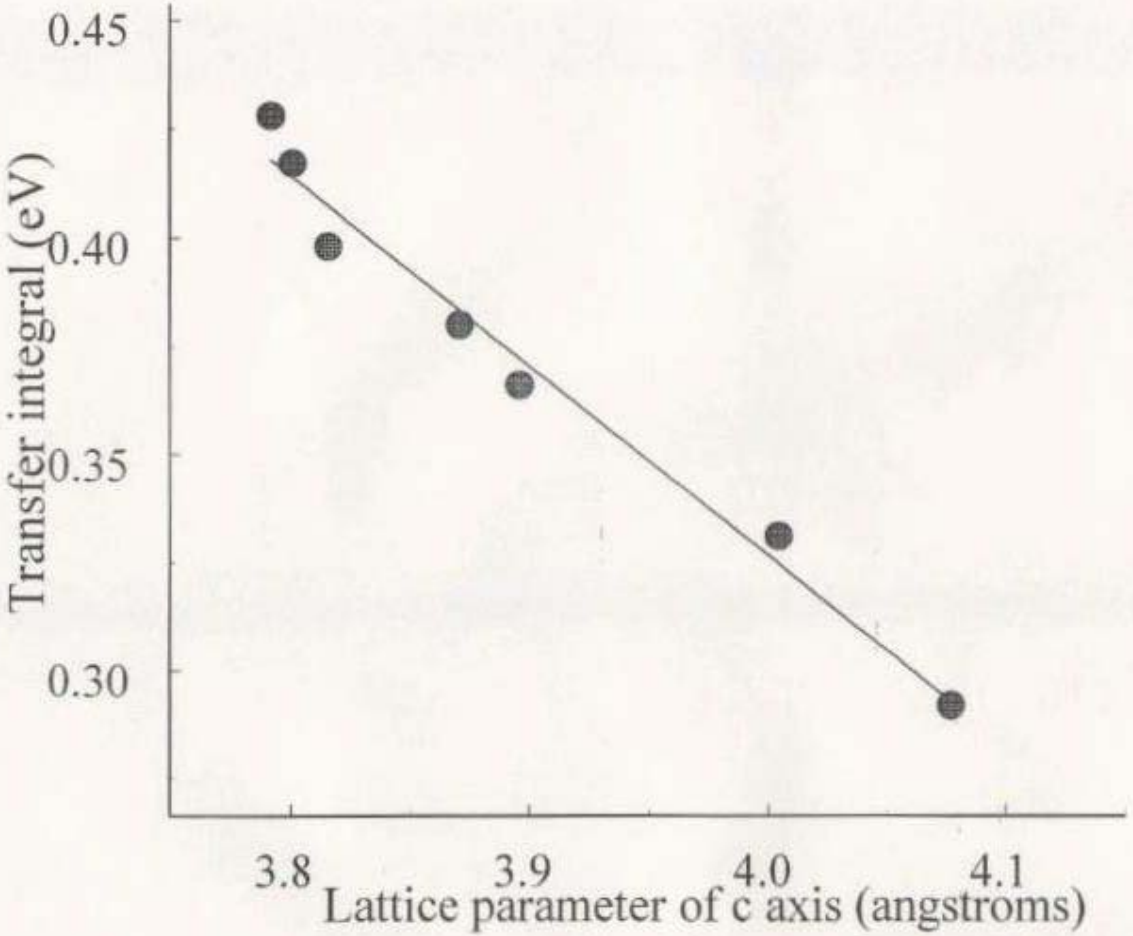

Fig. 3.2. Correlation between *t(2)* obtained from the HF/DZP calculations and the lattice parameters of the c axis.

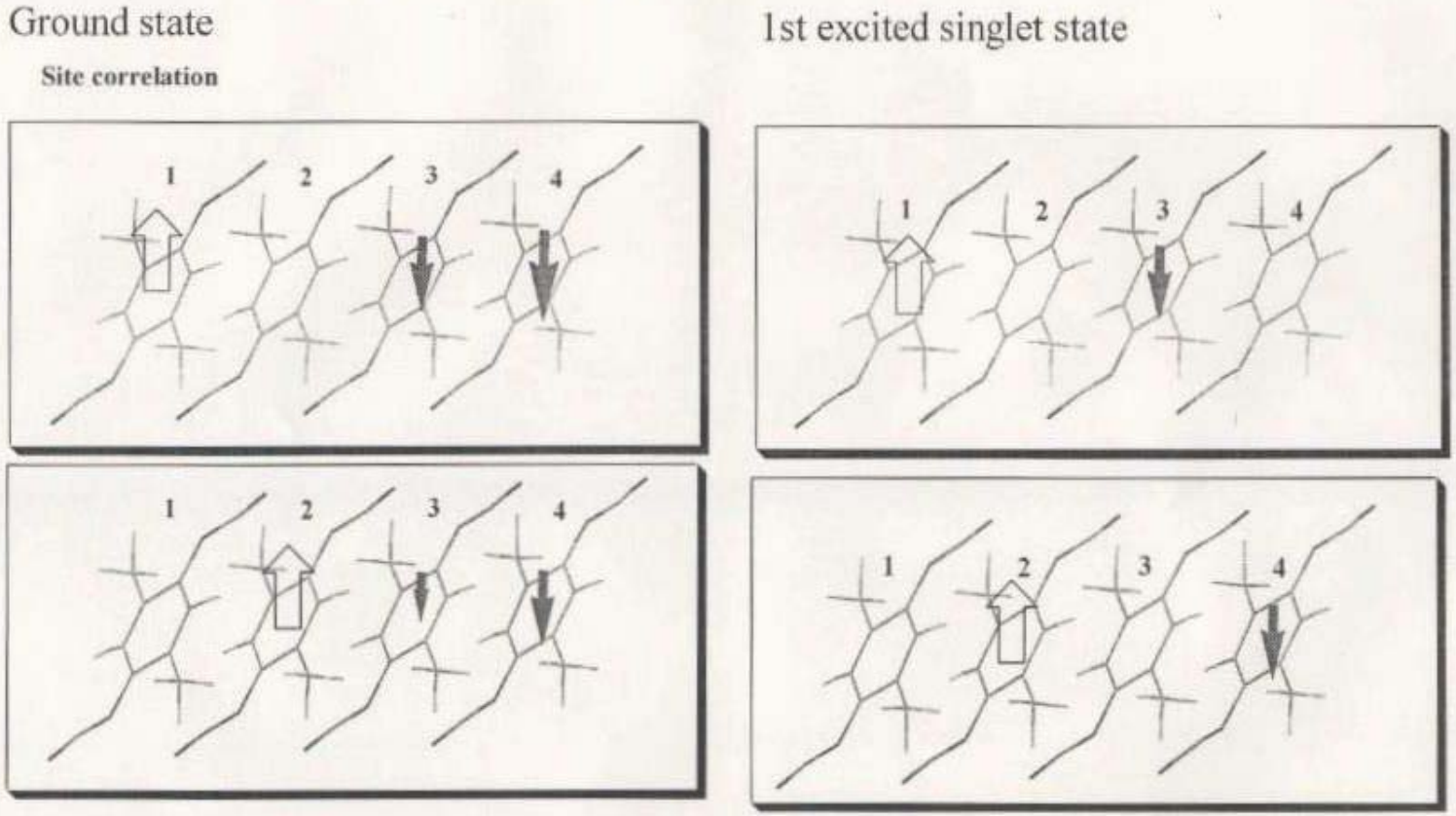

Fig. 3.3. The spin configurations of the ground state and 1st singlet excited state of finite tetramer model. Arrows pointing upwards (downwards) represent up (down) spins and solid arrows indicate the j' th LMO where spin correlation function (2.11) has strong amplitude toward the i' th LMO indicated by open arrows.

Ground state

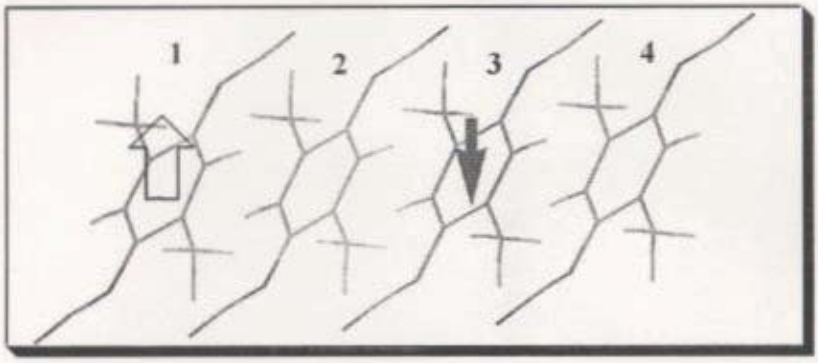

2 nd singlet excited state

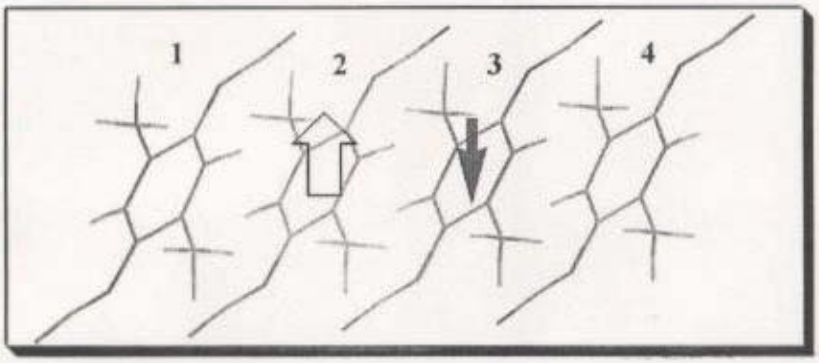

Fig. 3.4. The spin configurations of the ground state and the 2nd singlet excited state for the periodic tetramer model. The definitions of arrows follow those in Fig. 3.3.

Ground state

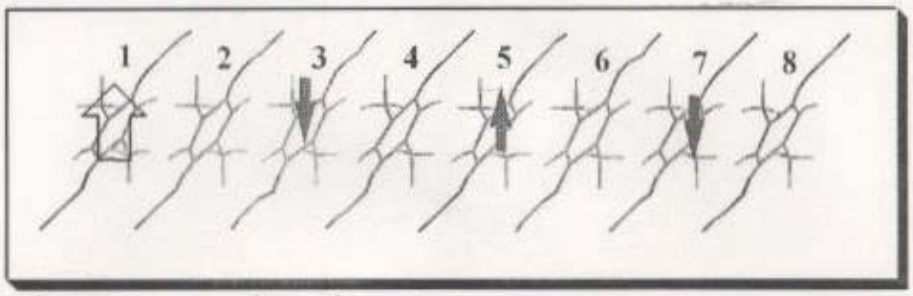

1st quintet excited state

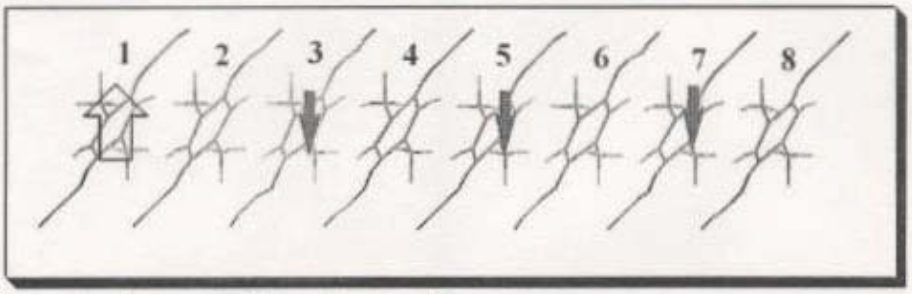

1st singlet excited state

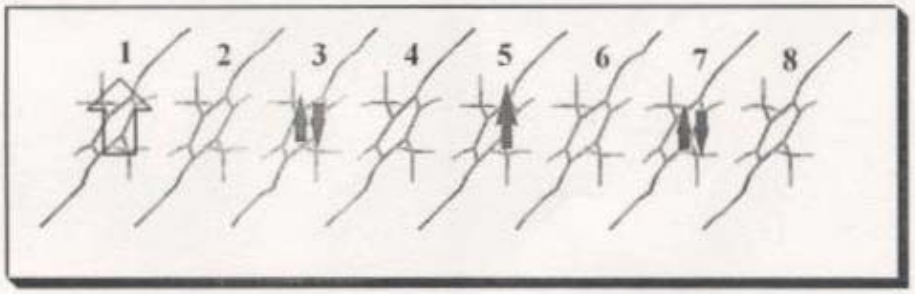

Fig. 3.5. The spin configurations of the ground state and some low-lying excited states for the anti-periodic octamer model. The definitions of arrows follow those in Fig. 3.3.

Table 3.1. Structural parameters (a-f: Å, g-h:degree) for R1,R2-DCNQI (R1=R2) molecules from the HF/DZP calculation.

R1	Charge	a	b	c	d	e	f	g	h
-H	0	1.141	1.345	1.274	1.477	1.476	1.330	120.1	176.6
-H	-1	1.151	1.323	1.329	1.437	1.435	1.359	119.0	176.3
-Cl	0	1.141	1.344	1.268	1.487	1.475	1.328	120.6	176.7
-Cl	-1	1.150	1.323	1.319	1.440	1.437	1.356	119.2	176.4
-Br	0	1.141	1.343	1.268	1.485	1.475	1.328	120.6	176.5
-Br	-1	1.150	1.323	1.319	1.438	1.437	1.355	119.2	176.3
-I	0	1.141	1.342	1.270	1.484	1.477	1.330	120.9	176.5
-I	-1	1.150	1.322	1.319	1.439	1.438	1.357	119.5	176.4
-Me	0	1.141	1.344	1.275	1.488	1.473	1.333	120.4	176.4
-Me	-1	1.151	1.321	1.330	1.443	1.435	1.361	119.4	176.1
-OMe	0	1.142	1.342	1.272	1.500	1.458	1.341	119.5	176.9
-OMe	-1	1.151	1.320	1.332	1.450	1.425	1.365	119.6	175.6

Table 3.2. Structural parameters (a-f: Å, g-h:degree) for R1,R2-DCNQI (R1=R2) molecules from experiments.

R1	Metal	Temperature	Charge	a	b	c	d	e	f	g	h
-Cl	Cu	RT[a,b]	-2/3	1.150	1.299	1.330	1.443	1.433	1.351	120.1	172.4
-Br	Cu	RT[b]	-2/3	1.152	1.306	1.329	1.434	1.443	1.350	120.6	172.4
-I	Cu	9K[c]	-2/3	1.154	1.322	1.336	1.445	1.432	1.362	121.1	172.5
-Me	Cu	20K[d]	-2/3	1.163	1.318	1.340	1.452	1.435	1.365	119.5	172.9
-OMe	Cu	RT[b]	-2/3	1.150	1.321	1.335	1.452	1.413	1.352	120.4	171.2
-H		e)	0	1.150	1.334	1.303	1.446	1.450	1.336	119.5	172.8

a) Room temperature. b) Reference 3. c) Reference 4. d) Reference 5. e) Reference 1.

Table 3.3. Structural parameters (a-f: Å, g-h:degree) for R1,R2-DCNQI $(R1=R2)^{-2/3}$ from the HF calculations with DZP basis set. (Average of neutral and anionic DCNQI molecules)

R1	a	b	c	d	e	f	g	h
-Cl	1.147	1.330	1.302	1.456	1.450	1.347	119.6	176.5
-Br	1.147	1.330	1.302	1.454	1.450	1.346	119.6	176.4
-I	1.147	1.329	1.303	1.454	1.451	1.348	120.0	176.4
-Me	1.148	1.329	1.312	1.458	1.447	1.352	119.7	176.2
-OMe	1.148	1.327	1.312	1.467	1.436	1.357	119.6	176.0

Table 3.4. Basis set dependence of structural parameters(a-f: Å, g-h:degree) for R1,R2-DCNQI(R1=R2) molecules from the HF calculations with SZ, DZ and DZP basis set.

R1	Basis set	Charge	a	b	c	d	e	f	g	h
-H	SZ	0	1.179	1.413	1.315	1.507	1.507	1.344	119.5	174.8
-H	DZ	0	1.155	1.346	1.286	1.475	1.473	1.338	124.2	175.4
-H	DZP	0	1.141	1.345	1.274	1.477	1.476	1.330	120.1	176.6
-H	SZ	-1	1.180	1.393	1.370	1.458	1.458	1.372	117.4	173.4
-H	DZ	-1	1.166	1.328	1.342	1.438	1.434	1.366	122.5	175.4
-H	DZP	-1	1.151	1.323	1.329	1.437	1.435	1.359	119.0	176.3
-Me	SZ	0	1.179	1.412	1.315	1.513	1.503	1.345	119.7	174.6
-Me	DZ	0	1.155	1.344	1.287	1.486	1.472	1.341	124.5	175.3
-Me	DZP	0	1.141	1.344	1.275	1.488	1.473	1.333	120.4	176.4
-Me	SZ	-1	1.180	1.391	1.369	1.461	1.456	1.372	117.7	173.3
-Me	DZ	-1	1.166	1.327	1.343	1.443	1.436	1.368	122.7	175.3
-Me	DZP	-1	1.151	1.321	1.330	1.443	1.435	1.361	119.4	176.1

Table 3.5. Transfer integrals and Coulomb interactions of (R1,R2-DCNQI)$_2$Cu salts (R1=R2) from the HF calculations.

	Temperature	Cluster	Charge	Basis set	Lattice parameter c (Å)	$t(1)$ (eV)	$t(2)$ (eV)	On-site Coulomb Interaction(eV)	Nearest-neighbor Coulomb interaction(eV)
DMe-DCNQI	RT [a]	Dimer	-1	SZ	3.871[c]		0.298	6.804	3.227
DMe-DCNQI	RT	Dimer	-1	DZ	3.871		0.362	6.424	3.276
DMe-DCNQI	RT	Dimer	0	DZP	3.871		0.365	6.390	3.224
DMe-DCNQI	RT	Dimer	-1	DZP	3.871	0.356	0.380	6.545	3.323
DMe-DCNQI	RT	Dimer	-2	DZP	3.871		0.373	6.357	3.326
DMe-DCNQI	RT	Dimer	-3	DZP	3.871		0.293	6.566	3.387
DMe-DCNQI	RT	Dimer	-4	DZP	3.871		0.273	6.382	3.265
DMe-DCNQI	100K	Dimer	-1	DZP	3.801[d]		0.417	6.536	3.362
DMe-DCNQI	20K	Dimer	-1	DZP	3.792[d]		0.428	6.529	3.367
DCl-DCNQI	RT	Dimer	-1	DZP	3.816[c]		0.398	6.433	3.334
DBr-DCNQI	RT	Dimer	-1	DZP	3.896[c]		0.366	6.431	3.305
DI-DCNQI	RT	Dimer	-1	DZP	4.077[e]		0.292	6.395	3.242
DI-DCNQI	9K	Dimer	-1	DZP	4.0042[e]	0.310	0.331	6.415	3.277
DMe-DCNQI	100K	Dimer	-1	SBK	3.801		0.422	6.510	3.349
DMe-DCNQI	100K	Trimer	-2	SBK	3.801		0.416	6.338, 6.282	3.332
(DMe-DCNQI)$_2$Cu	20K			Theory[b]		-0.25			
(DBr-DCNQI)$_2$Cu	RT			Theory[b]		-0.18			
(DI-DCNQI)$_2$Cu	9K			Theory[b]		-0.14			

a) Room temperature. b) Reference 7. c) Reference 3. d) Reference 5. e) Reference 4.

Table 3.6. Transfer integrals and Coulomb interactions for (R1,R2-DCNQI)$_2$X (X=Ag, Li) from the HF calculations.

	Temperature	Cluster	Charge	Basis set	Lattice parameter c (Å)	Transfer integral (eV)	On-site Coulomb Interaction (eV)	Nearest-neighbor Coulomb interaction(eV)
(DMe-DCNQI)$_2$Li	RT [a]	Tetramer	0	SBK	3.849[d]	0.368	6.265	3.240
(DMe-DCNQI)$_2$Li	RT	Tetramer	-2	SBK	3.849	0.374	6.233	3.283
(DI-DCNQI)$_2$Li	RT	Tetramer	0	SBK	4.076[e]	0.274	6.162	3.138
(DI-DCNQI)$_2$Li	RT	Tetramer	-2	SBK	4.076	0.226	6.156	3.131
(DMe-DCNQI)$_2$Ag	RT	Tetramer	0	SBK	3.818[f]	0.361	6.258	3.247
(DMe-DCNQI)$_2$Ag	RT	Tetramer	-2	SBK	3.818	0.370	6.227	3.283
(DMe-DCNQI)$_2$Cu	RT	Dimer	-1	DZP[b]	3.849[g]	0.380	6.545	3.323
(DI-DCNQI)$_2$Cu	RT	Dimer	-1	DZP[b]	4.077[d]	0.292	6.395	3.242
(DMe-DCNQI)$_2$Ag	RT			Theory[c]	3.818	-0.22		

a) Room temperature. b) Table 3.5. c) Reference 7. d) Reference 4. e) Reference 9. f) Reference 14. g) Reference 3.

Reference

[1] G. D. Andreetti, S. Bradamante, P. C. Bizzarri and G. A. Pagani, Mol. Cryst. Liq. Cryst. 120, 309 (1985).

[2] R. Kato, Y. Kashimura, S. Aonuma, H. Sawa, H. Takahashi and N. Mori, Mol. Cryst. Liq. Cryst. 143, 285 (1996).

[3] R. Kato, H. Kobayashi and A. Kobayashi, J. Am. Chem. Soc. 111, 5224 (1989).

[4] H. Sawa, private communication.

[5] K. Sinzger, S. Hünig, M. Jopp, D. Bauer, W. Bietsch, J. U. von Schütz, H. C. Wolf, R. K. Kremer, T. Metzenthin, R. Bau, S. I. Khan, A.Lindbaum, C. L. Lengauer and E. Tillmanns, J. Am. Chem. Soc. 115, 7696 (1993).

[6] T. Miyazaki and K. Terakura, Phys. Rev. B 56, R477 (1997).

[7] T. Miyazaki and K. Terakura, Phys. Rev. B 54, 10452 (1996).

[8] K. Hiraki and K. Kanoda, Phys. Rev. B 54, R17276 (1996).

[9] K. Hiraki, Doctoral thesis, The Graduate University for Advanced Studies (1997).

[10] H. Seo and H. Fukuyama, J. Phys. Soc. Jpn. 66, 1249 (1997).

[11] N. Kobayashi and M. Ogata, J. Phys. Soc. Jpn. 66, 3356 (1997).

[12] N. Kobayashi, M. Ogata and K. Yonemitsu, J. Phys. Soc. Jpn. 67, 1098 (1998).

[13] J. P. Pouget and S. Ravy, Synth. Met. 85, 1523 (1997).

[14] A. Kobayashi, private communication.

Chapter 4.

Geometrical and Electronic Structures of κ-BEDT-TTF Salts.

4.1 Geometrical structure and parameters of effective Hamiltonian

4.1.1 Molecular structure of BEDT-TTF

In the κ-(BEDT-TTF)$_2$[N(CN)$_2$]X (X=Cl, Br and I) crystals, each BEDT-TTF molecule has +1/2 charge according to their 3/4 filling. The optimized structural parameters of the BEDT-TTF$^{+1/2}$ monomers are shown in Table 4.1. We also show the XRD structural parameters of κ-(BEDT-TTF)$_2$[Cu(CN)$_2$]Br at 127 K [1] along with other averaged parameters of BEDT-TTF and BEDT-TTF' calculated by Demiralp and Goddard at HF/6-31G** [2]. Definitions of the carbon and sulfur sites are depicted in Fig. 1.4. We see that the deviations of our results from the XRD parameters are within 0.02 Å and 0.5 degrees in bond lengths and angles, respectively, except for R(C_3-C_3) and θ(S_2-C_3-C_3). Two reasons are considerable for the deviations. One is the effect of neglecting the anion layer. The other is that the XRD structural parameters of the -CH_2-CH_2- group have an ambiguity since BEDT-TTF molecules can take the staggered and eclipsed conformations as shown in Fig. 1.4. Demiralp and Goddard show the energy difference between the conformations is very small, i.e., 0.0032 kcal/mol at HF/6-31G** and suggested the possibility that BEDT-TTF molecule can take both structures even at 10 K [3]. Our optimized structure also agrees with their calculation.

4.1.2 HOMO and LUMO

The HOMO and LUMO of the BEDT-TTF molecule are drawn in Fig. 4.1. The used structural parameters are taken from the XRD experiment of κ-(BEDT-TTF)$_2$Cu[N(CN)$_2$]Br. The anti-bonding character of -S_1-C_1- and -S_1-C_2- and bonding character of -C_1-C_1- and -C_2-C_2- are observed in HOMO. The HOMO coefficients of p-type orbitals in -C_1-S_1-C_2- are large whereas those of -S_2-C_3- are small. In the crystal, the formal charge of BEDT-TTF is +1/2 and the p-type orbitals of -C_1-S_1-C_2- contribute to the conductivity of BEDT-TTF crystals.

4.1.3 Ionization potential

The calculated vertical and adiabatic ionization potentials (IPs) are shown in Table 4.2, where IP(1) and IP(2) denote those from the Koopmans theorem and from the ΔSCF method, respectively. Our vertical IP(1) is overestimated, compared with the experimental one, 6.21 eV [4], since the orbital relaxation is neglected in IP(1). On the other hand, the vertical and adiabatic IPs(2) are underestimated. The dependence of the basis set is small in both IPs.

4.1.4 Parameters of effective Hamiltonian

In Table 4.3, we show transfer integrals and Coulomb interactions derived from cluster calculations. The transfer integrals are defined in Fig. 1.5. The sign of transfer integral, $t(2)$, depends on taking phases of wave function. For κ-(BEDT-TTF)$_2$Cu[N(CN)$_2$]Cl, on-site and nearest-neighbor Coulomb interactions are calculated to be 5.90 and 3.25 eV, respectively. These Coulomb interactions are bare and larger than the effective ones [5]. $t_{b1}(1)$ and $t_{b1}(2)$ are calculated as 0.274 and 0.280 eV. The difference is small, so that the orbital relaxation hardly affects the transfer integrals in the κ-(BEDT-TTF)$_2$Cu[N(CN)$_2$]X system. For X= Cl and Br, $t_{b1}(1)$ are 0.274 and 0.266, respectively. This ordering indicates the strength of dimerization, which is consistent with the Kanoda's diagram in Fig. 1.6. Basically, our transfer integrals are consistent with the previous results of Fortunelli and Painelli at HF/6-31G** [6]. However, the ab initio transfer integral, $t_p(2)$, −0.1584 eV for X= Br is larger than the semiemprical one, −0.101 eV, obtained by the extended Hückel calculation [7]. t_{b2} is a little smaller than the semiemprical one.

4.1.5 Fermi surface and band dispersion

Within the tight-binding approximation, we calculate the band dispersions and Fermi surfaces for X=Cl and Br using three transfer integrals, $t_{b1}(2)$, $t_{b2}(2)$ and $t_p(2)$, obtained by ab initio MO calculations based on the XRD structures at 127 K. The

results are shown in Figs. 4.2 and 4.3, respectively. The gap between the upper (anti-bonding) two bands and the lower(bonding) two bands for X= Cl, is larger than that for X=Br. The calculated Fermi surface of X= Br is very similar to that for X= Cl. Our theoretical Fermi surface is consistent with the experimental one of the κ-(BEDT-TTF)$_2$Cu[N(CN)$_2$]Cl salt obtained by the angle-dependent magnetoresistance oscillation (ARMO) and Shubnikov-de Haas oscillation experiments under pressure [8]. We find that the ratio of the closed part around the Z point in the Fermi surface is 20.7 % for the κ-(BEDT-TTF)$_2$Cu[N(CN)$_2$]Cl salt, which is close to the experimental one, 16-18 % [9,10]. The Fermi surface and band dispersion are also consistent with first-principles ones calculated by Xu *et al.* based on LDA [11]. On the other hand, the ratio is calculated to be 26.2 % with semiempirical transfer integrals [7].

4.2 Electron correlation

4.2.1 Model Hamiltonian and HF approximation

In this calculation, we choose a 2-D extended Hubbard model at 0 K to elucidate the role of long-range Coulomb interaction. The model is shown in Fig. 4.4. The circle represents BEDT-TTF monomer. We use the one- and two-electron interactions calculated for the κ-(BEDT-TTF)$_2$Cu[N(CN)$_2$]Br salt at 127 K. The transfer integrals, $t_{b1}(2)$, $t_{b2}(2)$ and $t_p(2)$, and on-site Coulomb interaction in Table 4.3 are used and $t_q(2)$ is neglected. The long-range Coulomb interactions are shown in Table 4.4. Since Kino and Fukuyama have already discussed the effect of the intradimer transfer integral, t_{b1}, based on the HF model [5], we fix the ab initio transfer integrals and concentrate on the role of Coulomb interaction.

We first study the effect of on-site Coulomb interaction, U, changing U as a variable from 0 to 1.2 eV with neglecting V_{ij}. In Fig. 4.5, the absolute value of spin moment per molecule, <Sz>, is drawn as a function of U. In the region $0 < U < 0.7$ eV, the ground state is a paramagnetic metal. The hole density (ρ_h) is close to +0.5 at each site. In the region $0.7 < U < 0.95$ eV, the HF calculations did not converge due to quasi-degeneracy. At U = 0.95 eV, the system becomes an AF insulator. The configuration of spin alignments with Sz(A)=Sz(B) and Sz(C)=Sz(D) is shown in the inset of Fig. 4.5. Since the direction of the spin moment of dimer 1 and that of dimer 2 are opposite, the AF ordering occurs between dimers. ρ_h is close to +0.5 at each site. The spin moment becomes about 0.4 μ_B per BEDT-TTF molecule. This magnitude of spin moment agrees with the experimentally observed one in the AF ordered state, 0.4 - 1.0 μ_B per dimer [12]. As U increases, the spin moment becomes large and finally saturated. These results are consistent with the previous results by Kino and Fukuyama, and Demiralp and Goddard who also applied the HF approximation to the 2-D Hubbard model for κ-(BEDT-TTF)$_2$Cu(NCS)$_2$ salt.

Then, we change intradimer Coulomb interaction, V_{int}, from 0 to 1.0 eV for U = 0.7 and 0.9 eV. The absolute value of spin moment per molecule, <Sz >, is shown as a

function of V_{int} in Fig. 4.6. In the case of U =0.9 eV, the ground state is an AF insulator in the entire range, $0 < V_{int} < 1.0$ eV. The AF spin configuration is almost the same as in Fig. 4.5. The magnitude of spin moment increases slightly as V_{int} becomes larger. In the case of U =0.7 eV, the ground state is the paramagnetic state for $0 < V_{int} < 0.14$ eV. However, when $V_{int} = 0.14$ eV, the AF insulator has a lower energy. We check the contribution of transfer integrals, U and V_{int} to the HF total energies. The Fock term of V_{int} is found to mainly stabilize the AF insulator.

Using the isolated dimer, we evaluate the effective on-site Coulomb interaction on the dimer, U_{dimer}, defined as E(2)+E(0)–2E(1), where E(n) is the total energy of the dimer with n electron(s). We derive the total energy of the Hamiltonian,

$$H = \varepsilon \sum_{i,\sigma}^{2} a_{i\sigma}^{+} a_{i\sigma} - t_{b1} \sum_{\sigma} (a_{1\sigma}^{+} a_{2\sigma} + a_{2\sigma}^{+} a_{1\sigma}) + \sum_{i}^{2} U n_{i\uparrow} n_{i\downarrow} + V_{int} n_1 n_2 , \tag{4.1}$$

considering all spin configurations where ε is the orbital energy of BEDT-TTF HOMO. The indices, 1 and 2, represent different BEDT-TTF molecules in the dimer. The total energies of the lowest states with 1 and 2 electrons and U_{dimer} are given by,

$$E(2) = 2\varepsilon + \frac{1}{2}(U + V_{int}) - \frac{1}{2}(U - V_{int})\sqrt{1 + (\frac{4t_{b1}}{U - V_{int}})^2} , \tag{4.2}$$

$$E(1) = \varepsilon - t_{b1} , \tag{4.3}$$

$$\begin{aligned} U_{dimer} &= E(2) + E(0) - 2E(1) \\ &= 2t_{b1} + \frac{1}{2}(U + V_{int}) - \frac{1}{2}(U - V_{int})\sqrt{1 + (\frac{4t_{b1}}{U - V_{int}})^2} . \end{aligned} \tag{4.4}$$

U_{dimer} are calculated to be 0.29 and 0.66 eV for two sets of parameters, $V_{int} = 0$ eV, U = 0.9 eV and $V_{int} = 0.5$ eV, U = 0.9 eV, respectively. We show U_{dimer} as a function of V_{int} in Fig. 4.7. This indicates that V_{int} enhances U_{dimer} and supports our HF results.

Next, we inspect the nearest-neighbor Coulomb interaction, V_{NN}. The value of charge disproportionation, δ (deviation from the average value, 1.5) and the magnitude of spin moment per molecule, <Sz>, as a function of V_{NN} in Fig. 4.8. The parameter, V_{NN} is changed from 0 to 0.5 eV with U= 0.9 eV and $V_{int} = 0.5$ eV. In the range of 0 <

$V_{NN} < 0.14$ eV, the ground state is an AF insulator with spin moment, ~0.41 μ_B. At V_{NN} = 0.14 eV, the ground state becomes the charge ordering (CO) state. The charge disproportionation δ of A and B sites are 0.47 and those of C and D are −0.47 at V_{NN} = 0.2 eV.

We change the two parameters, next-nearest-neighbor Coulomb interaction, V_{NNN}, and nearest-neighbor Coulomb interaction, V_{NN}, with U= 0.9 eV and V_{int}= 0.5 eV. The phase diagram of V_{NNN} and V_{NN} is shown in Fig. 4.9. In the range, $0 < V_{NN} < 0.1$ eV and $0 < V_{NNN} < 0.4$ eV, the ground state is the AF insulator. At V_{NN} = 0.15 eV and V_{NNN}= 0 eV, the CO state has a lower energy. In the range, $0.3 < V_{NN} < 0.4$ eV and $0.3 < V_{NNN} <$ 0.4 eV, the ground state is the paramagnetic metal. Since the unit cell includes only two BEDT-TTF dimers, we can not describe the orderings whose periodicities are larger than that of the unit cell, though other ordering states might have lower energies. However, Poilblanc *et al.* calculated the ground state of the 1-D extended Hubbard model by the exact diagonalization method and also found that its ground state is the paramagnetic metal in a certain range of Coulomb interactions [13] similar to the present case.

As was shown in chapter 2, the dimer model offers a reasonable description of the κ-(BEDT-TTF) salts. Based upon this fact, we employ infinite half-filled square-lattice models to approximate the 2-D extended Hubbard model at strong coupling,

$$H = \sum_i U n_{i\uparrow} n_{i\downarrow} + \sum_{i,j \in NNsite} V_1 n_i n_j + \sum_{i,j \in NNNsite} V_2 n_i n_j, \tag{4.5}$$

where NNsite and NNNsite represent the nearest-neighbor and next-nearest-neighbor sites, respectively, and U, V_1 and V_2 are the on-site, nearest-neighbor and next-nearest-neighbor Coulomb interactions, respectively. In this model, we neglect transfer integrals. Two spin configurations, which correspond to the obtained AF and CO states are shown in Fig 4.10. The unit cell is drawn by the dash line. Using the equation (4.5), the energy per unit cell of both models are calculated to be $4V_1 + 4V_2$, $U + 8V_2$. The CO configuration is stabilized for $V_1 > V_2 + U/4$ whereas the AF spin configuration is more

stable for $V_1 < V_2 + U/4$. Actually, as shown in the phase diagram, the ground state is the CO state in the range, $V_{NN} > V_{NNN} + U/4$ and the ground state is the AF state in the range, $V_{NN} < V_{NNN} < 0.2$.

4.2.2 Exact diagonalization study of decamer under the periodic condition.

We study electron correlation of the H_{eff} extracted from transformed UMO integrals of κ-(BEDT-TTF)$_2$Cu[N(CN)$_2$]Br salt. The one-electron interactions, t_{mn_1} and t_{mn_2}, defined in Fig. 4.11 are calculated to be –0.114 eV and –0.045 eV, respectively. The $\langle mm \mid mm \rangle$, $\langle mn_1 \mid mn_1 \rangle$, $\langle mn_2 \mid mn_2 \rangle$ and $\langle mn_3 \mid mn_3 \rangle$ are 4.55, 1.88, 1.65 and 1.14 eV, respectively.

We calculate the ground state of $H_{eff}(1)$ and analyze its spin correlation function. The ground state has the CO correlation as drawn in Fig. 4.12. The spin correlation function, $\Delta_{1\uparrow,i\uparrow}(i = 3,5,7,9)$, and $\Delta_{1\uparrow,i\downarrow}(i = 1,3,5,7,9)$ are 2.00. The other $\Delta_{1\uparrow,i\sigma}$ are less than 0.01. This implies that the localization is strong. On the other hand, the ground state of $H_{eff}(2)$, has the AF correlation as drawn in Fig. 4.13. The spin correlation function, $\Delta_{1\uparrow,i\uparrow}(i = 3,5,7,9)$ and $\Delta_{1\uparrow,6\downarrow}$ are close to 1.30 and $\Delta_{1\uparrow,i\downarrow}(i = 2,4,8,10)$ are close to 1.47. The other $\Delta_{1\uparrow,i\sigma}$ are less than 0.75. This ordering is in consistent with the experimental one. These results indicate that the next-nearest-neighbor Coulomb interactions are important to reproduce the AF ordering correctly.

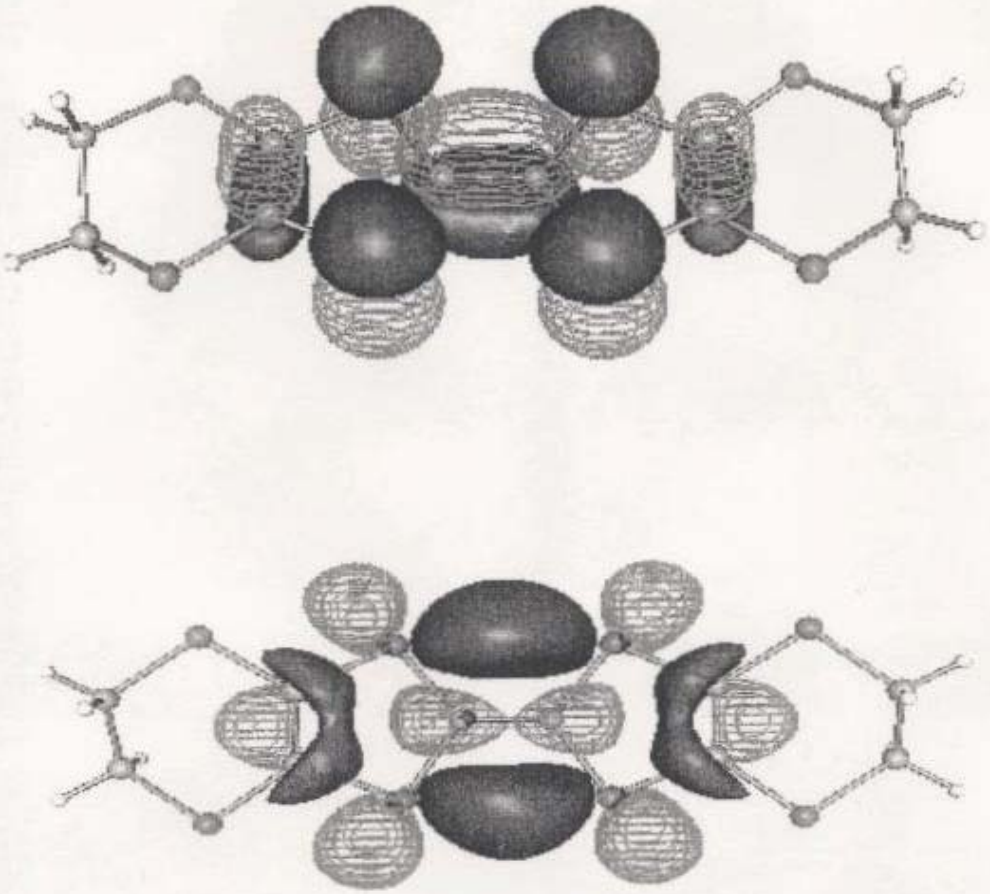

Fig. 4.1. HOMO (top) and LUMO (bottom) of the BEDT-TTF molecule at HF/DZP with $q_s = +1$.

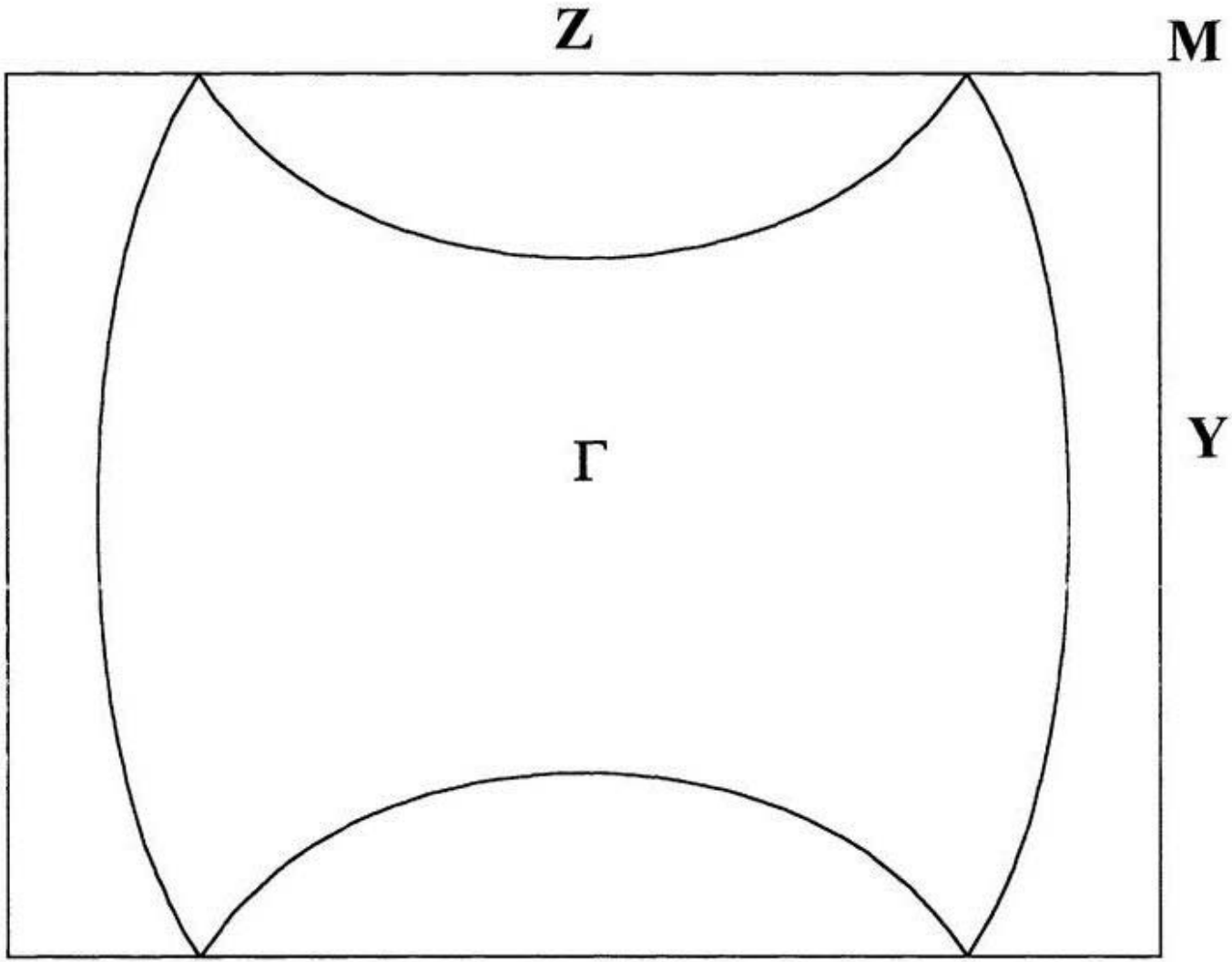

Fig. 4.2. Fermi surface of κ-$(BEDT\text{-}TTF)_2Cu[N(CN)_2]Cl$.

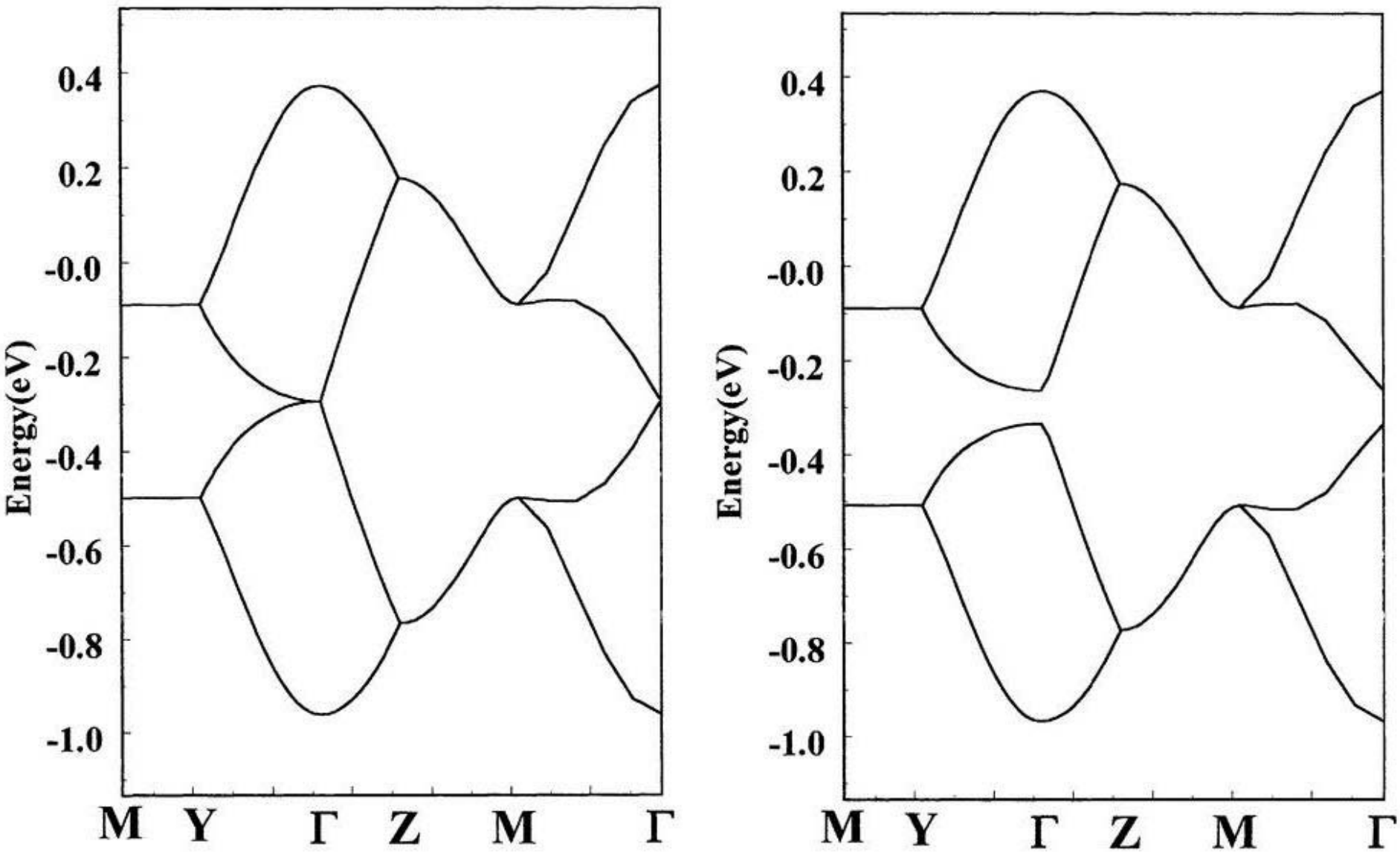

Fig. 4.3. The calculated band structures of X=Br (left) and X=Cl (right).

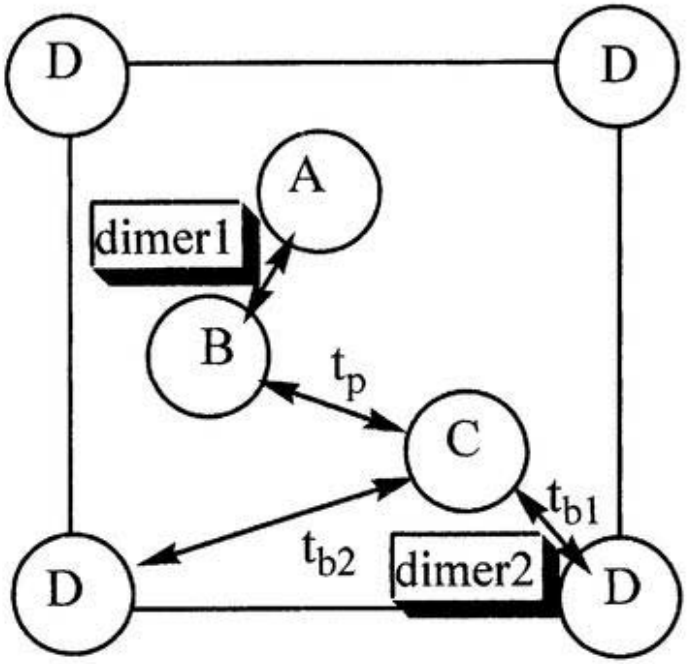

Fig. 4.4. The model of κ-(BEDT-TTF)$_2$Cu[N(CN)$_2$]X (X=Cl, Br, I).

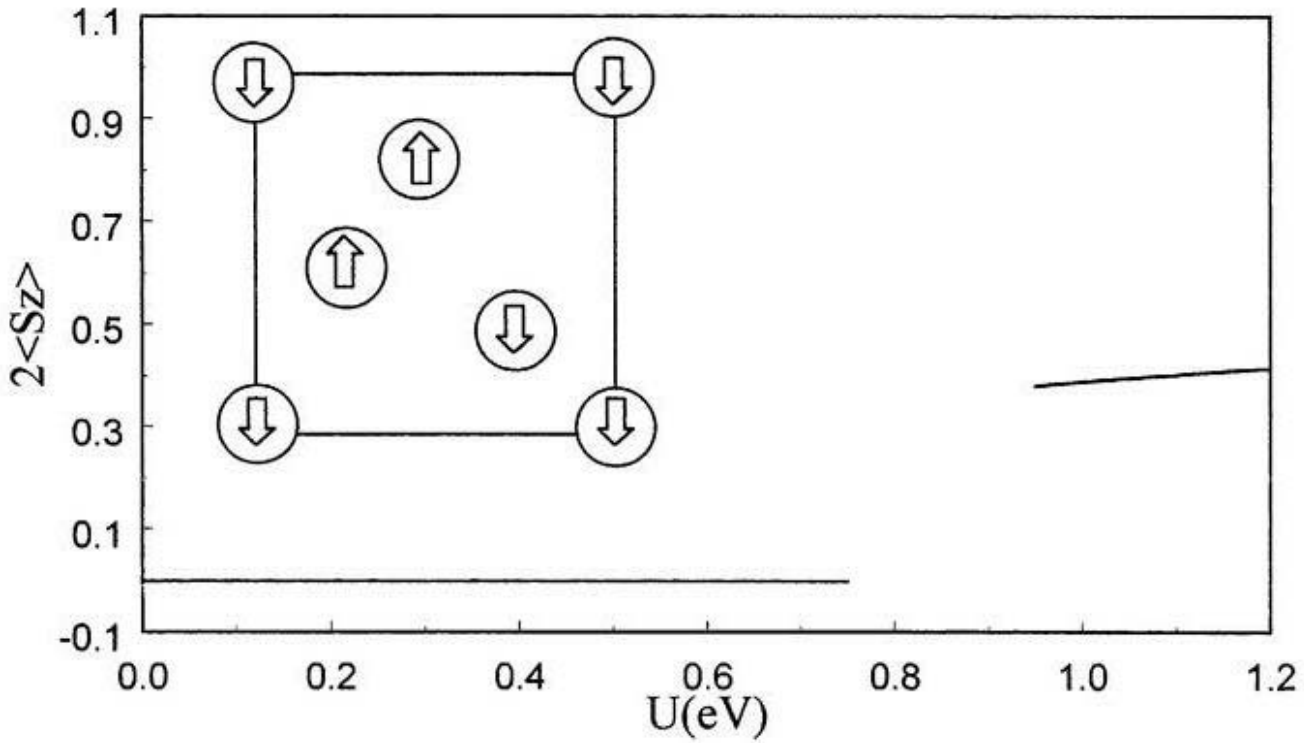

Fig. 4.5. The U dependence of magnetic moment, <Sz>. The inset shows the alignment of spin moments. Arrows pointing upwards (downwards) represent up (down) spins.

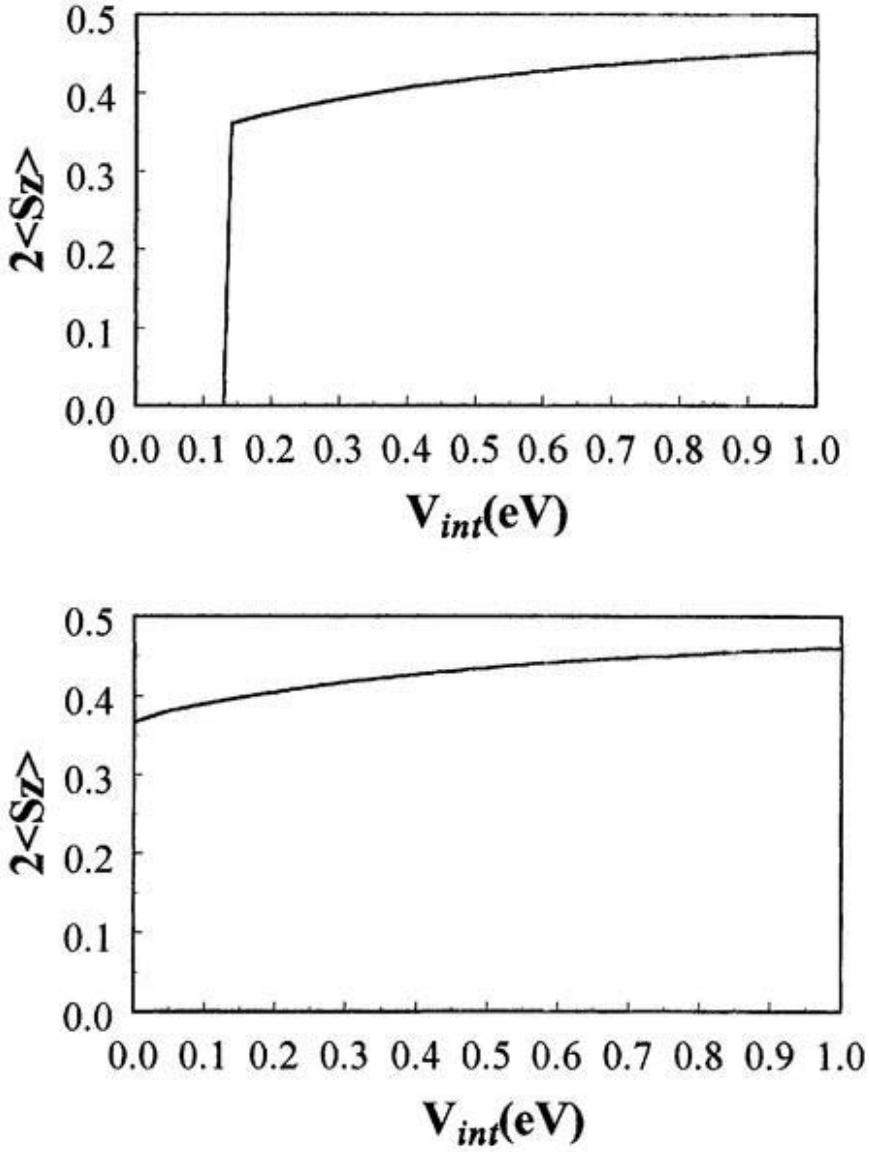

Fig. 4.6. The Vint dependence of magnetic moment, <Sz>. Here, the top figure is for U =0.7 eV, whereas the bottom one for U= 0.9 eV.

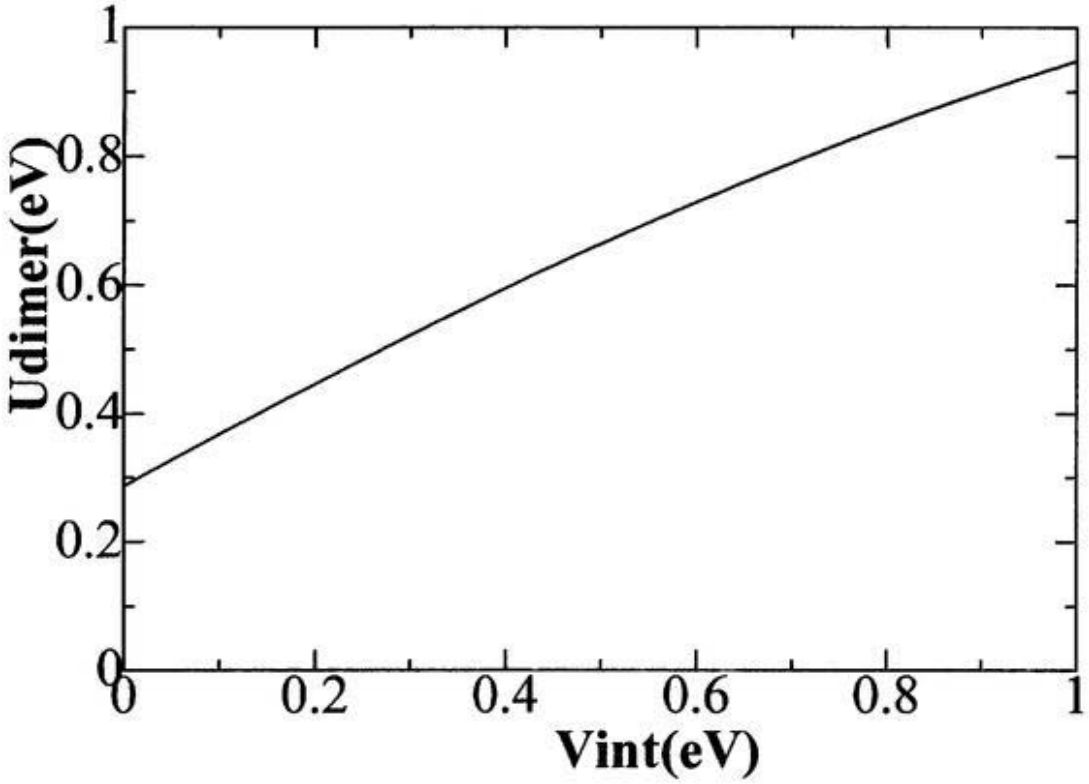

Fig. 4.7. The Vint dependence of U_{dimer} with U = 0.9 eV.

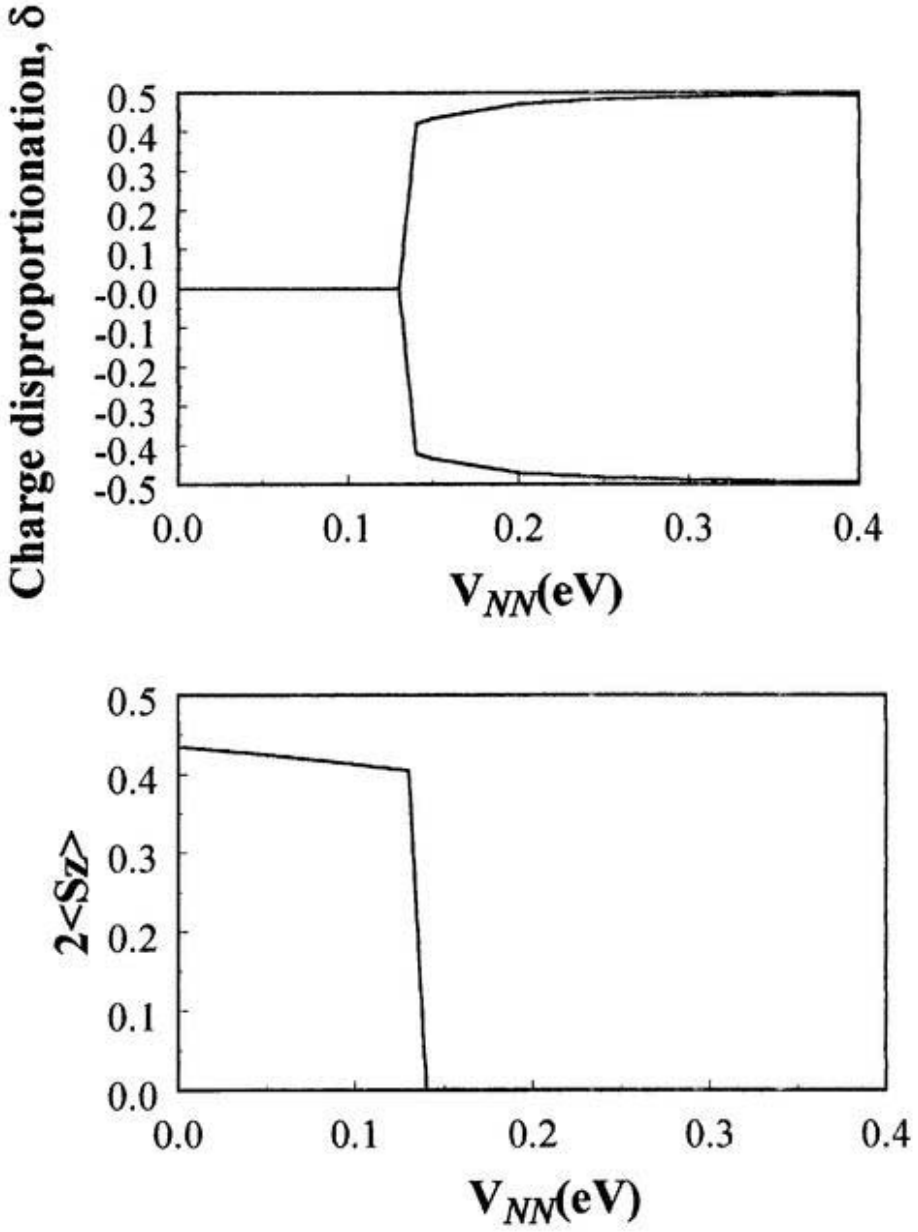

Fig. 4.8. The V_{NN} dependence of magnetic moment, <Sz> (top) and charge disproportionation, δ (bottom) with U =0.9eV and V_{int}=0.5eV.

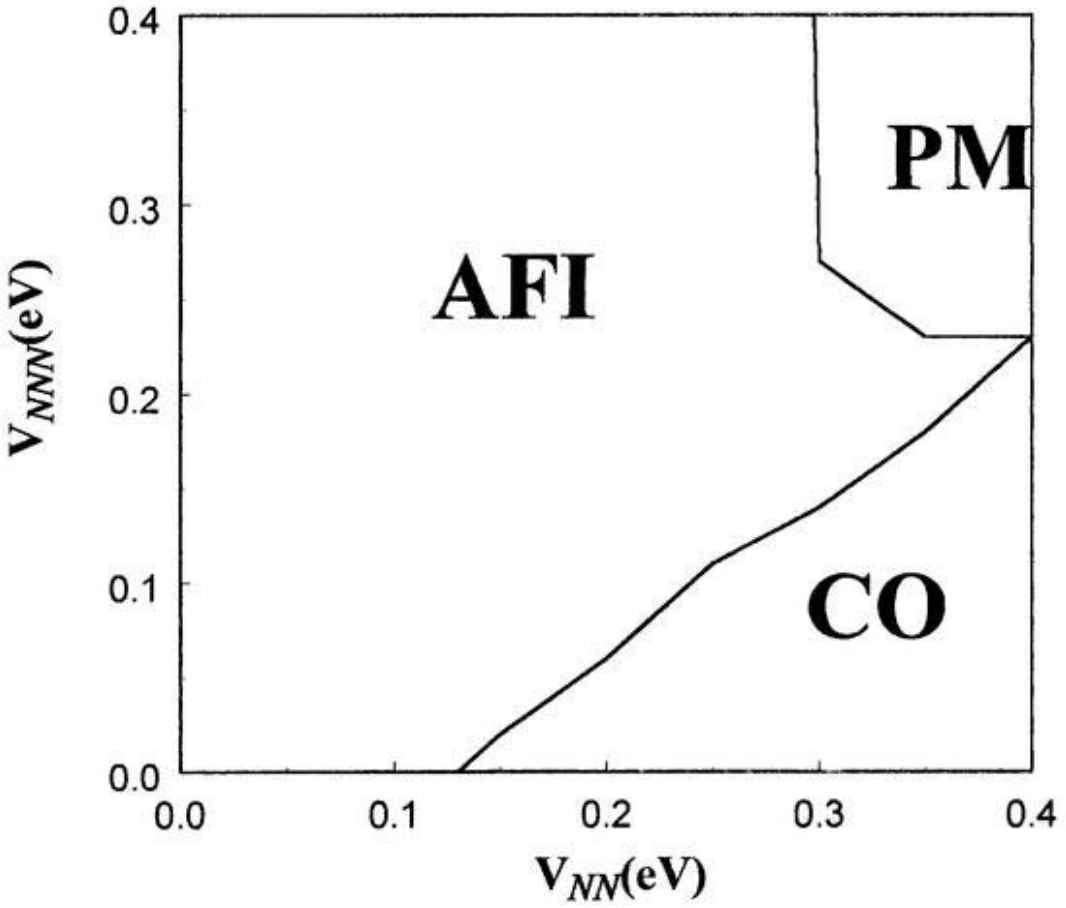

Fig. 4.9. The phase diagram as a function of V_{NN} and V_{NNN} with U =0.9 eV and V_{int}=0.5eV. Here, AFI, PM and CO represent the antiferromagnetic insulator, paramagnetic metal and charge ordering states, respectively.

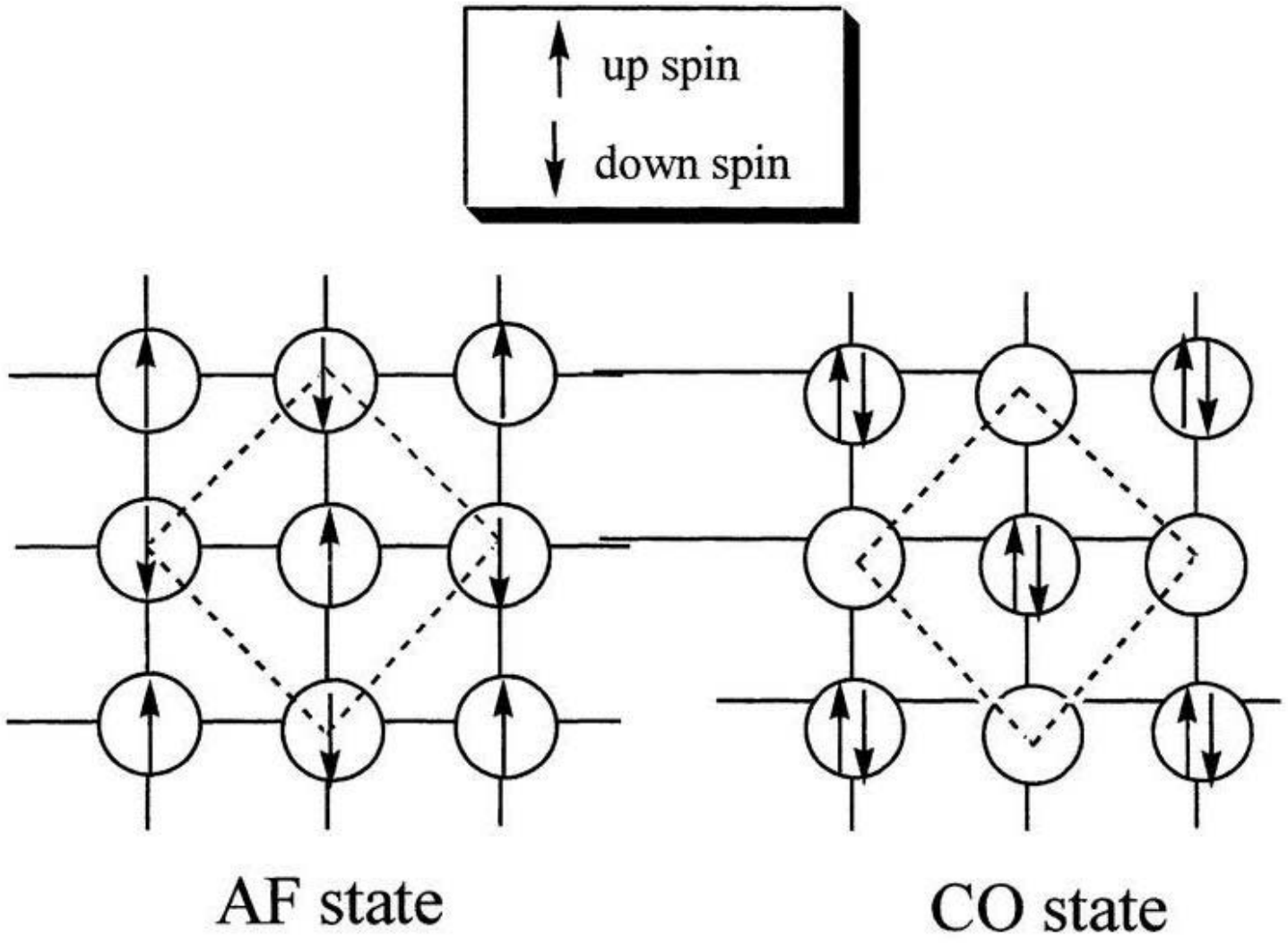

Fig. 4.10. Spin configurations in the antiferromagnetic (AF) and charge ordering (CO) states.

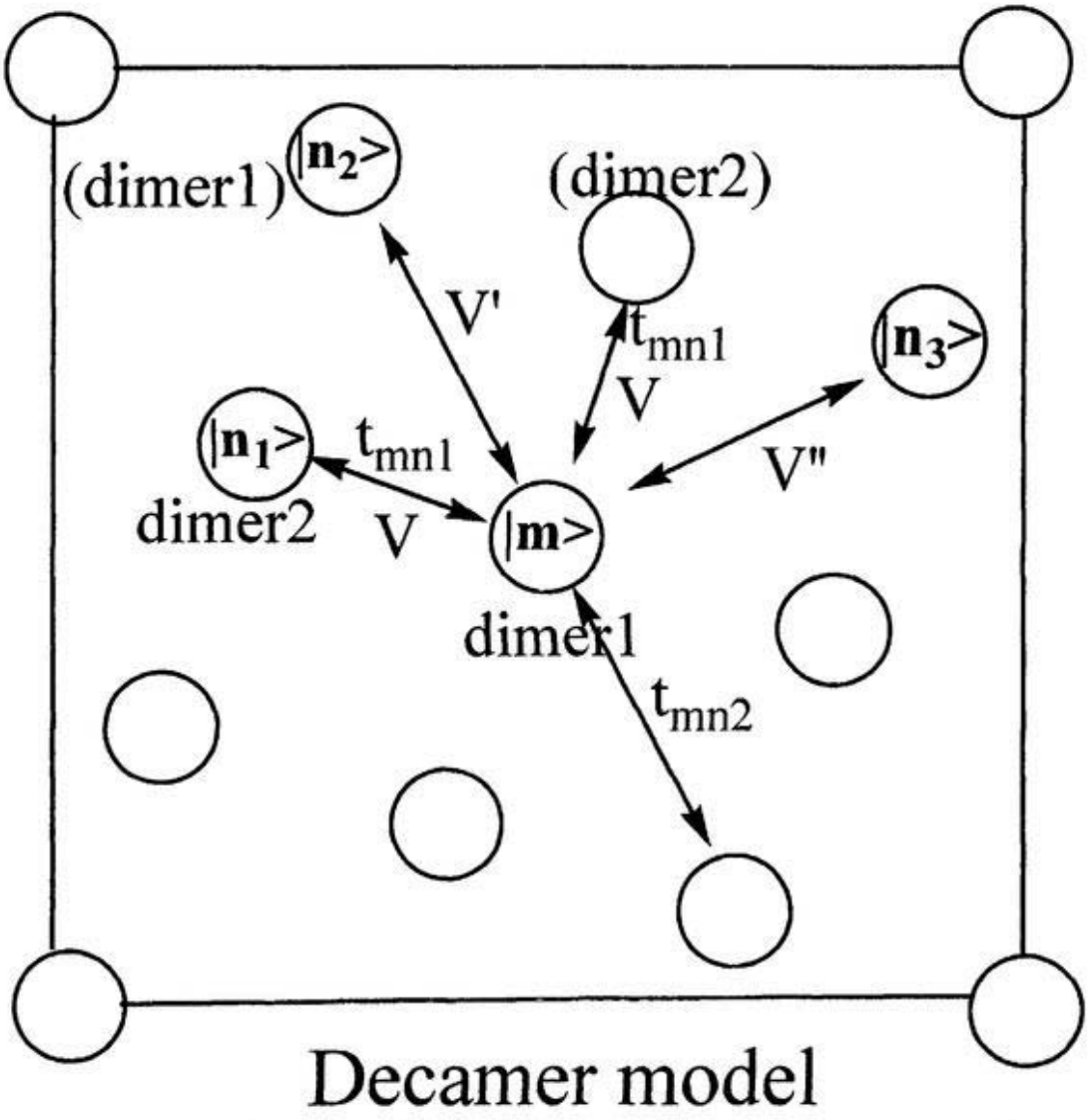

Fig. 4.11. The definitions of transfer integrals and Coulomb interactions.

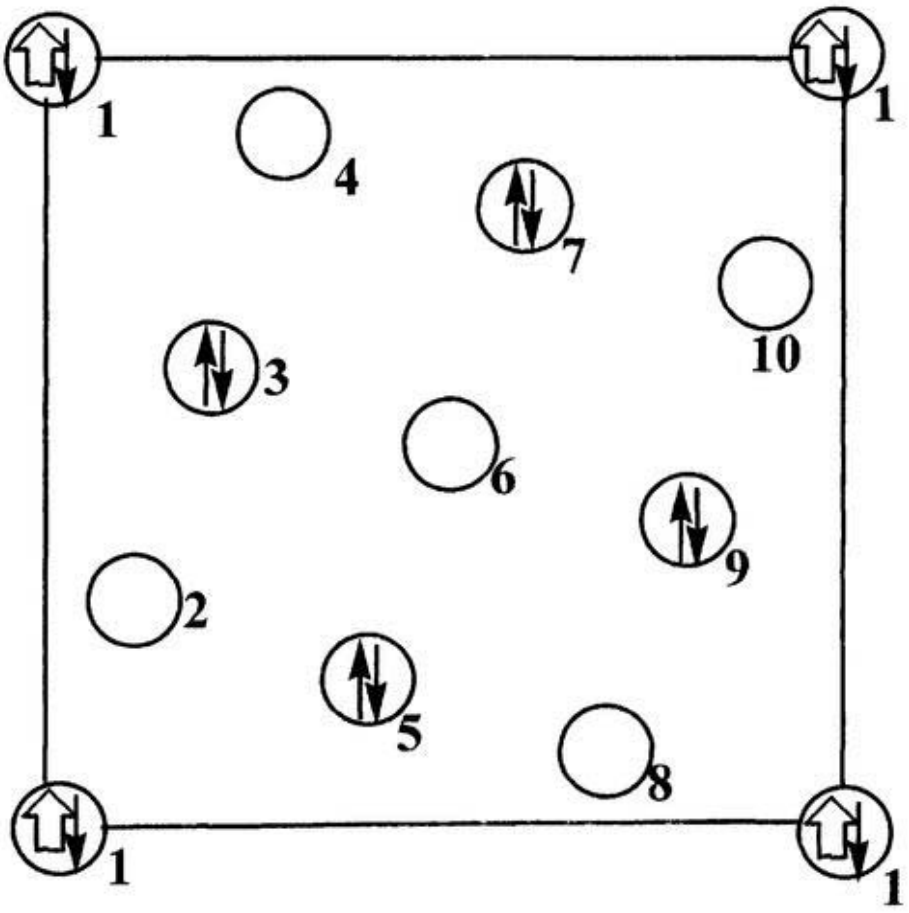

Fig. 4.12. The spin configuration of the ground state of $H_{eff}(1)$. The definitions of arrows follow those in Fig. 3.3.

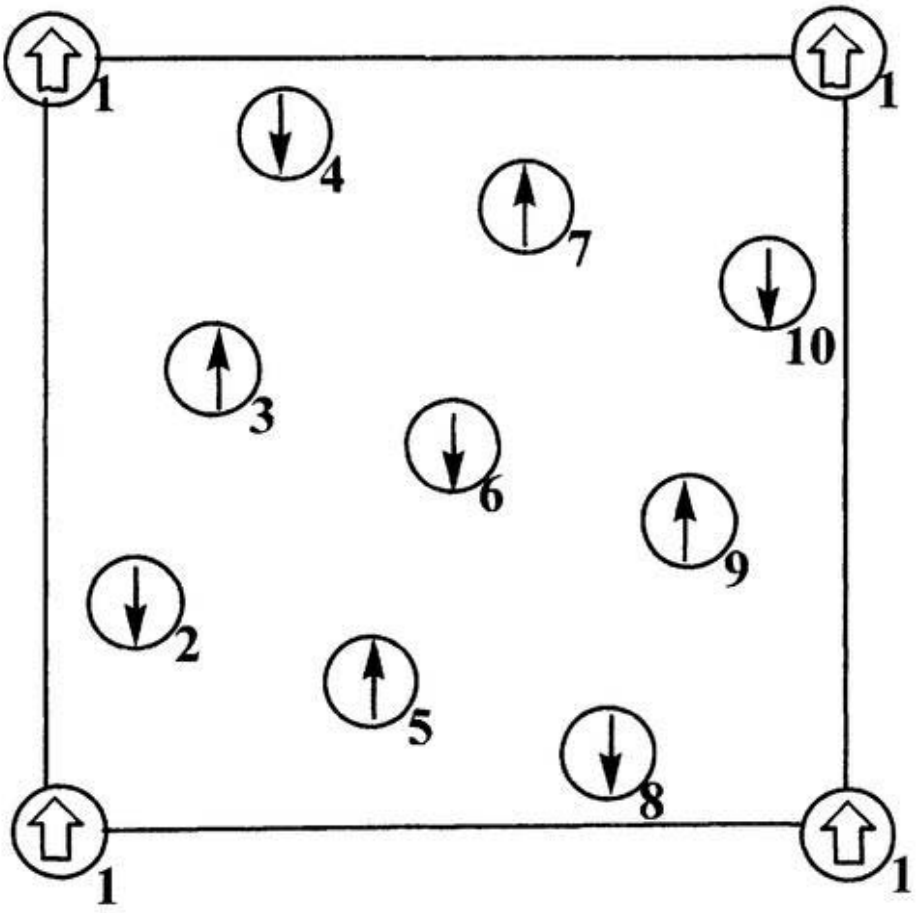

Decamer model

Fig. 4.13. The spin configuration of the ground state of $H_{eff}(2)$. The definitions of arrows follow those in Fig. 3.3.

Table 4.1. Structural parameters of BEDT-TTF$^{+1/2}$ from the HF/DZP calculations.

	Theory Present	Theory[a]	Expt[b]
Distance (Å)			
$R(C_1=C_1)$	1.355	1.358	1.360
$R(C_1-S_1)$	1.746	1.747	1.741
$R(S_1-C_2)$	1.758	1.761	1.751
$R(C_2=C_2)$	1.333	1.329	1.343
$R(C_2-S_2)$	1.763	1.767	1.749
$R(S_2-C_3)$	1.811	1.814	1.811
$R(C_3-C_3)$	1.527	1.524	(1.485)
Angle(degree)			
$\theta(C_1=C_1-S_1)$	122.9	123.0	122.4
$\theta(C_1-S_1-C_2)$	95.9	96.0	95.1
$\theta(S_1-C_2=C_2)$	117.0	117.0	117.1
$\theta(C_2=C_2-S_2)$	128.7	128.8	128.9
$\theta(C_2-S_2-C_3)$	100.9	100.7	100.9
$\theta(S_2-C_3-C_3)$	113.0	112.8	

a) Average structural parameters of BEDT-TTF and BEDT-TTF$^+$. Reference 2.

b) κ-$(BEDT\text{-}TTF)_2Cu[N(CN)_2]Br$ Reference 1.

Table 4.2. Ionization potential (eV) from the HF/DZP calculations.

	IPV[a]	IPA[b]
IP(1) at HF/DZP	6.82	
IP(1) at HF/SBK+31G*	6.83	
IP(1)[c]	6.87	
IP(2) at HF/DZP	6.11	5.83
IP(2) at HF/SBK+ 31G*	6.15	5.82
IP(2)[c]		5.77
Experiment [d]		6.21

a) Vertical ionization potential b) Adiabatic ionization potential

c)Reference 2. d)Reference 4.

Table 4.3. Transfer integrals and Coulomb interactions (eV) for $(BEDT\text{-}TTF)_2Cu[(CN)_2]X$ (X=Cl, Br, I) from the HF/SBK+31G*(dimer) and HF/SBK-31G(tetramer) calculations.

	Charge (tetramer)	Temperature	On-site Coulomb	Nearest-neighboring Coulomb	t_{b1}((1) (eV)	t_{b1}(2) (eV)	t_{b2}(2) (eV)	t_p(2) (eV)	t_q(2) (eV)
$(ET)_2Cu[N(CN)_2Cl]$	+0	127 K	5.9004	3.2503	0.2743	0.2804	0.0717	-0.1584	-0.0319
$(ET)_2Cu[N(CN)_2Br]$	+0	127 K	5.9025	3.2270	0.2657	0.2687	0.0643	-0.1669	-0.0260
$(ET)_2Cu[N(CN)_2Br]$	+2	127 K					0.0418	-0.1504	-0.0001
$(ET)_2Cu[N(CN)_2I]$	+0	127 K	5.8346	3.2198	0.2392	0.2438	0.0484	0.1610	-0.0162
$(ET)_2Cu[N(CN)_2I]$	+0	295 K	5.8332	3.1913	0.2328	0.2362	0.0513	-0.1480	-0.0235
$(ET)_2Cu[N(CN)_2Br]$[a]		127 K				-0.301	-0.080	-0.135	-0.047
$(ET)_2Cu[N(CN)_2Br]$[b]		RT [c]				0.244	0.092	0.101	-0.034

a) q_d=0 , HF level Reference 6. b) Extend Hückel approximation. Reference 7. c) Room temperature

Table 4.4. Coulomb interactions (eV) of the κ-(BEDT-TTF)$_2$Cu[N(CN)$_2$]X (X=Cl, Br, I) salts at HF/SBK-31G with q_d=0.

	X=Cl	X=Br	X=I
V2	2.428	2.441	2.409
V3	1.428	1.419	1.438
V4	1.529	1.528	1.520
V5	2.160	2.164	2.177
V6	2.139	2.113	2.071
V7	1.640	1.629	1.592
V8	1.247	1.238	1.216
V9	1.389	1.406	1.408
V10	1.118	1.121	1.136
V11	0.909	0.905	0.923

Reference

[1] U. Geiser, A. J. Schultz, H. H. Wang, D. M. Watkins, D. L. Stupka, J. M. Williams, J. E. Schirber, D. L. Overmyer, D. Jung, J. J. Novoa and M. -H. Whangbo, Physica C 174, 475 (1991).

[2] E. Demiralp and W. A. Goddard III, J. Phys. Chem. 98, 9781 (1994).

[3] E. Demiralp, S. Dasgupta and W. A. Goddard III, J. Am. Chem. Soc. 117, 8154 (1995).

[4] N. Sato, G. Saito and H. Inokuchi, Chem. Phys. 76, 79 (1983).

[5] H. Kino and H. Fukuyama, J. Phsy. Soc. Jpn. 64, 2726 (1995).

[6] A . Fortunelli and A. Painelli, J. Chem. Phys. 106, 8051 (1997).

[7] T. Komatsu, N. Matsukawa, T. Inoue and G. Saito, J. Phys. Soc. Jpn. 65, 1340 (1996).

[8] Y. Yamauchi, M. V. Kartsovnik, T. Ishiguro, M. Kubota and G. Saito, J. Phsy. Soc. Jpn. 65, 354(1996).

[9] T. Sasaki, H. Sato and N. Toyata, Solid State Commun. 76, 507 (1990).

[10] K. Oshima, T. Mori, H. Inokuchi, H. Urayama, H. Yamochi and G. Saito, Phys. Rev B 38, 938 (1988).

[11] Y. -N. Xu, W. Y. Ching, Y. C. Jean and Y. Lou, Phys. Rev. B 52, 12946 (1995).

[12] K. Miyagawa, A. Kawamoto, Y. Nakazawa and K. Kanoda, Phys. Rev. Lett. 75, 1174 (1995).

[13] D. Poilblanc, S. Yunoki, S. Maekawa and E. Dagotto, Phys. Rev. B. 56, R1645 (1997).

Chapter 5.

Conclusion

We studied the electronic properties of DCNQI-Cu,Ag,Li and κ-(BEDT-TTF)$_2$Cu[N(CN)$_2$]X (X=Cl, Br, I) salts. We calculated the geometrical and electronic structures of DCNQI monomers at HF/DZP. The structures predicted from theory are in good agreement with experimental ones. We calculated the oligomers to obtain transfer integrals, on-site Coulomb interactions and so on. A clear correlation between the lattice parameters of the c axis and theoretical transfer integrals is discovered. Using ab initio parameters, we constructed the effective Hamiltonian of tetramer and octamer models for the DCNQI-Ag/Li salts. In both models, the ground state has the AF and charge ordering correlations which correspond to the $2k_F$ SDW and $4k_F$ CDW states. In the octamer model, we observed that the spin correlation is weak. The ground state and some low-lying excited states have the correlation of charge ordering which corresponds to the $4k_F$ CDW state observed experimentally for the 1-D DCNQI salts.

We calculated the geometrical and electronic structures of BEDT-TTF monomers at HF/DZP. The optimized structure well reproduces the experimental one except the ethylene group. Transfer integrals was calculated and compared with experimental results and the other theoretical ones. Using the ab initio transfer integrals, we drew Fermi surface and band dispersions of κ-(BEDT-TTF)$_2$Cu[N(CN)$_2$]X (X=Br, Cl). For X=Cl, the gap between the upper (anti-bonding) two bands and the lower (bonding) two bands is larger than that for X=Br. To study the role of the long-range Coulomb interactions, we calculated the ground state of a 2-D extended Hubbard model within the HF approximation. Then we found that the intradimer Coulomb interaction, V_{int}, has a function to enhance the effective on-site Coulomb interaction on the dimer (U_{dimer}), which is attributed to the transition between paramagnetic metal and AF state. We drew phase diagram as a function of representative nearest-neighbor and next-nearest-neighbor dimer Coulomb interactions, V_{NN} and V_{NNN}, respectively. The ground states are the AF insulator, charge ordering state and paramagnetic metal depending on the ratio of V_{NN} and V_{NNN}. When V_{NN} is larger than some critical value in the absence of V_{NNN}, the ground state is the charge ordering state. On the other hand, when V_{NNN} is larger than

V_{NN}, the ground state is the AF insulator or paramagnetic metal. Thus, we conclude that it is necessary to consider enough ranges of long-range Coulomb interactions to calculate the electronic properties.

To study the effect of long-range Coulomb interactions, we use two methods; exact diagonalization of effective Hamiltonian derived from quantum chemistry calculations and the HF approximation of model Hamiltonian. The former method is explicit within the given effective Hamiltonian. However, it requires huge computational sources. Actually, the treated model is at most decamer at the half filling in this study. It is necessary to use large cluster models to investigate long-range Coulomb interactions. The latter one does not require computational sources so much. However, the applicability of this method is still limited. Therefore the obtained results were discussed carefully. We hope that our HF results will be also studied by a well-defined quantitative method in future.

Acknowledgements

The author has enjoyed staying at the Graduate University for Advanced Studies for three years and would like to acknowledge people who supported, influenced, and encouraged me during the course of this study.

The author expresses his sincere gratitude to Prof. Yoshitaka Tanimura for the sincere supervision at the Graduate University for Advanced Studies. The author would like to express his sincere thanks to Prof. Kenji Yonemitsu and Dr. Seiichiro Ten-no for their valuable discussions, comments and suggestions. The author wished to thank all the members of the Tanimura and Yonemitsu research groups, especially, Dr. J. Kishine, Dr. M. Mori, Dr. T. Ogawa, Dr. M. Kuwabara, Dr. T. Taniguchi, Dr. K. Miyazaki, Dr. Y. Maruyama, Mr. O. Hino for stimulating discussions and encouragement. The author also thanks Prof. H. Sawa, Prof. H. Kobayashi, Prof. A. Kobayashi, Prof. K. Kanoda, Dr. K. Hiraki for giving experimental data. The author feels thankful to the Japan Society for the Promotion of Science for financial support.

The author also expresses his sincere thanks to his parents for their encouragement and financial support.